State Feedback Controller Design of an Active Suspension System for Vehicles Using Pole Placement Technique

A. Wéber, M. Kuczmann

Széchenyi István University, Department of Automation
Egyetem tér 1., 9026, Győr
E-mail: mandycandy.art@gmail.com

Abstract: The paper presents a method for designing a state feedback controller of an active suspension system of a quarter car model. This is a survey based on a specific example. The designed controller of the active suspension system improves the driving control, safety and stability, because during the ride, the periodic swinging motion generated by the road irregularities on wheels can be decreased. This periodic motion damages the driving comfort, and may cause traffic accidents. The state feedback controller is designed to stand road induced displacements. Computer simulations of the designed controller have been performed in the frame of Scilab and XCos.

Keywords: state feedback, pole placement, active suspension system

1. Introduction

Many researches performed on active suspension system have been presented in the recent years leading to more sophisticated regulatory approaches such as linear (fuzzy [1] PID controller [2]) and nonlinear control systems (artifical neural network controllers [3]). The active suspension system is a mechatronic suspension [4] and is important for improving the ride comfort. Because of the adverse impacts caused by road imbalances, the wheel can lose contact with the road, it can not deliver force,

and therefore the driving of the vehicle becomes uncertain. The periodic swinging motion can damage the driving comfort, the car parts, the cargo, and this motion can generate health damage, too. The primary purpose of the active suspension system is to minimize the vertical displacement of the vehicle and guarantee road maintenance. For modeling and simulation, a quarter car model has been chosen (see Fig. 1).
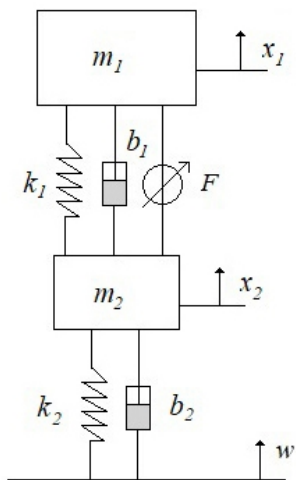

Figure 1. Quarter car model

2. Mathematical modeling

2.1. The quarter car model

Dynamic systems are described by several scientific and engineering branches and are modeled by state equations. Using differential equations, the operation of complicated dynamic systems can be modeled with relatively high precision. For defining the state

variables of a quarter car model the Euler-Lagrange equation is used [5]:

$$\frac{d}{dt}\frac{\partial K}{\partial \dot{x}} - \frac{\partial K}{\partial x} + \frac{\partial P}{\partial x} + \frac{\partial R}{\partial \dot{x}} = F. \tag{1}$$

The equation is described by the kinetic energy K, the potential energy P and the Rayleigh distribution R, as follows [6]:

$$K = \frac{1}{2}m_1\dot{x}_1^2 + \frac{1}{2}m_2\dot{x}_2^2, \tag{2}$$

$$P = \frac{1}{2}k_1(x_1 - x_2)^2 + m_1gx_1 + \frac{1}{2}k_2(x_2 - w)^2 + m_2gx_2, \tag{3}$$

$$R = \frac{1}{2}b_1(\dot{x}_1 - \dot{x}_2)^2 + \frac{1}{2}b_2(\dot{x}_2 - \dot{w})^2, \tag{4}$$

where
m_1- sprung mass;
m_2- un-srpung mass;
k_1- suspension stiffness;
k_2- tire stiffness;
b_1,b_2- damping coefficients;
F- action control force;
x_1- car body displacement;
x_2- wheel displacement;
w- road induced displacement.

2.2. State-space representation of a quarter car model

After obtaining the partial derivatives and substituting them into the Euler-Lagrange equation, the following equations are obtained:

$$m_1\ddot{x}_1 + k_1(x_1 - x_2) + m_1g + b_1(\dot{x}_1 - \dot{x}_2) = F, \tag{5}$$

$$m_2\ddot{x}_2 - k_1(x_1 - x_2) + k_2(x_2 - w) + m_2 g - b_1(\dot{x}_1 - \dot{x}_2) + b_2(\dot{x}_2 - \dot{w}) = -F. \quad (6)$$

The mathematical state of a dynamic system is described by the state variables. State variables often relate to a physical process in engineering systems, where the correlation needed to store mass, pulse and current are to be calculated.

The state variables define a state-space. In this state-space, the state vector $x(t)$ is specified. The movement of the system is the displacement of its end point [7]. A state-space representation is a mathematical model of a physical system in control engineering. This is a set of input, output and state variables related by first-order differential equations.

The states of the present system are defined as follows: $\dot{x}_1 = x_3$, $\ddot{x}_1 = \dot{x}_3$. Four state variables are defined for the system:

$$\dot{x}_1 = x_3, \quad (7)$$

$$\dot{x}_2 = \frac{b_1}{m_2} x_1 - \frac{b_1}{m_2} x_2 - \frac{b_2}{m_2} x_2 + \frac{b_2}{m_2} w + x_4, \quad (8)$$

$$\dot{x}_3 = \left(\frac{b_1^2}{m_1 m_2} - \frac{k_1}{m_1} \right) x_1 - \left(\frac{b_1^2}{m_1 m_2} + \frac{b_1 b_2}{m_1 m_2} - \frac{k_1}{m_1} \right) x_2 - \frac{b_1}{m_1} x_3$$
$$+ \frac{b_1}{m_1} x_4 + \frac{b_1 b_2}{m_1 m_2} w + \frac{1}{m_1} f - g, \quad (9)$$

$$\dot{x}_4 = \frac{k_1}{m_2} x_1 - \frac{k_1}{m_2} x_2 - \frac{k_2}{m_2} x_2 + \frac{k_2}{m_2} w - \frac{1}{m_2} f - g. \quad (10)$$

In the case of a linear system, the general form [8] of the state variable equations are:

$$\dot{x} = Ax + Bu, \quad (11)$$

$$y = Cx + Du. \tag{12}$$

Here, x is the state vector, u and y are the column vector containing exitations and responses. A is the system matrix, B, C and D matrices contain the appropriate coefficient [9].

The state-space representation of a quarter car model is described as follow:

$$
\begin{bmatrix} \dot{x}_1 \\ \dot{x}_2 \\ \dot{x}_3 \\ \dot{x}_4 \end{bmatrix} = \begin{bmatrix} 0 & 0 & 1 & 0 \\ \frac{b_1}{m_2} & -\left(\frac{b_1}{m_2} + \frac{b_2}{m_2}\right) & 0 & 1 \\ \left(\frac{b_1^2}{m_1 m_2} - \frac{k_1}{m_1}\right) & -\left(\frac{b_1^2}{m_1 m_2} + \frac{b_1 b_2}{m_1 m_2} - \frac{k_1}{m_1}\right) & -\frac{b_1}{m_1} & \frac{b_1}{m_1} \\ \frac{k_1}{m_2} & -\left(\frac{k_1}{m_2} + \frac{k_2}{m_2}\right) & 0 & 0 \end{bmatrix} \begin{bmatrix} x_1 \\ x_2 \\ x_3 \\ x_4 \end{bmatrix}
$$
$$
+ \begin{bmatrix} 0 & 0 & 0 \\ 0 & \frac{b_2}{m_2} & 0 \\ \frac{1}{m_1} & \frac{b_1 b_2}{m_1 m_2} & -g \\ -\frac{1}{m_2} & \frac{k_1}{m_2} & -g \end{bmatrix} \begin{bmatrix} F \\ w \\ 1 \end{bmatrix}. \tag{13}
$$

The performance parameters of the vehicle are given in Table 1. [6]. After substituting the values, the state-space representation as follow:

$$
\begin{bmatrix} \dot{x}_1 \\ \dot{x}_2 \\ \dot{x}_3 \\ \dot{x}_4 \end{bmatrix} = \begin{bmatrix} 0 & 0 & 1 & 0 \\ 12.5 & -40.5 & 0 & 1 \\ -59.482759 & 11.206897 & -1.7241379 & 1.7241379 \\ 587.5 & -5337.5 & 0 & 0 \end{bmatrix} \begin{bmatrix} x_1 \\ x_2 \\ x_3 \\ x_4 \end{bmatrix}
$$
$$
+ \begin{bmatrix} 0 & 0 & 0 \\ 0 & 28 & 0 \\ 0.0034483 & 48.275862 & -9.81 \\ -0.025 & 4750 & -9.81 \end{bmatrix} \begin{bmatrix} F \\ w \\ 1 \end{bmatrix}. \tag{14}
$$

The output variable of the quarter car model is as follows:

$$y = \begin{bmatrix} 1 & 0 & 0 & 0 \end{bmatrix} \begin{bmatrix} x_1 \\ x_2 \\ x_3 \\ x_4 \end{bmatrix} + \begin{bmatrix} 0 & 0 & 0 \end{bmatrix} \begin{bmatrix} F \\ w \\ 1 \end{bmatrix}. \tag{15}$$

Table 1. Parameters

Parameters	Value	Unit
m_1	290	kg
m_2	40	kg
k_1	23500	N/m
k_2	190000	N/m
b_1	500	N/m/s
b_2	1220	N/m/s
g	9.81	m/s^2

3. Simulations of the quarter car model

3.1. Full state feedback

Controllability is an important property of a controlled plant. The system can be controlled when the rank of controllability matrix M_c is maximal, i.e. the matrix is invertible if the determinant of the matrix is not zero [10]. The Kalman's controllability matrix looks as follow ($n = 4$):

$$M_c = \begin{bmatrix} b & Ab & A^2b & ... & A^{n-1}b \end{bmatrix}, \tag{16}$$

$$M_c = \begin{bmatrix} 0 & 0.0034483 & -0.0490488 & -0.4007186 \\ 0 & -0.025 & 1.0556034 & 92.098313 \\ 0.0034483 & -0.0490488 & -0.4007186 & 248.99601 \\ -0.025 & 0 & 135.46336 & -5663.0995 \end{bmatrix}. \tag{17}$$

After determining the controllability matrix, Ackermann's pole placement can be used because the state transformation and the feedback matrix can be directly given [6]. Because the system is controllable, Ackermann's pole placement is used for the state feedback. Ackermann's formula is a control design method for solving the pole allocation problem.
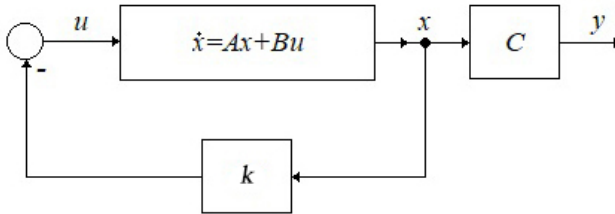

Figure 2. State feedback in continuous time

The task is to move the system's egienvalues to new places in the closed loop system. This is the pole placement, which is why the state feedback k is to be determined, (see Fig. 2 [10]). The polynomial of a closed loop system in general case is

$$\lambda^n + p_1 \lambda^{n-1} + p_2 \lambda^{n-2} ... + p_n = 0. \tag{18}$$

When using the pole placement method, the eigenvalues are changed, as it can be written as:

$$\phi_{cl}(\lambda) = |\lambda E - (A - Bk^T)| = 0. \tag{19}$$

The eigenvalues of the original system as follows:

$$\lambda = \begin{bmatrix} -20.40805 & +70.147933i \\ -20.40805 & -70.147933i \\ -0.7040194 & +8.4630446i \\ -0.7040194 & -8.4630446i \end{bmatrix}. \tag{20}$$

The new poles are selected as:

$$p = \begin{bmatrix} -200 & -30 & -30 & -30 \end{bmatrix} \qquad (21)$$

and the gain vector has been designed by Ackerman's formula,

$$k = \begin{bmatrix} 237767.73 & -221169.83 & 32173.44 & -5473.3186 \end{bmatrix}. \qquad (22)$$

Using the pole placement method, the new eigeinvalues of the system are as follows:

$$\lambda = \begin{bmatrix} -200 \\ -30.001573 \\ -29.999214 & +0.0013619i \\ -29.999214 & -0.0013619i \end{bmatrix}. \qquad (23)$$

3.2. Simulating the system

To realize simulations Scilab program with XCos interface has been used. In the simulation two cases have been examined; the first when the displacement induced by the road is zero, the second when this displacement is 50 mm. There simulations are analysed with and without the designed control.

3.2.1. Modeling without controller

If $w = 0$, then the gravitational force is pressed for the car body (see Fig. 3) and this showed that, the system left alone is set to a stationarity state after some swing. In case of $w = 50$ mm jump, car body displacement is affected by road induced displacement (see Fig. 4), the system initially leaving it goes out of the steady state for 10 seconds when it reaches a pothole, causing mass m_1 to swing movement, 10 seconds after the transient section becomes steady state. It can be seen that this value is 50 mm higher.

3.2.2. Modeling with controller

In case when there is no road induced displacement, but there is a controller (see Fig. 5), it can be seen the swings are eliminated, the stationary state is smoother. By the
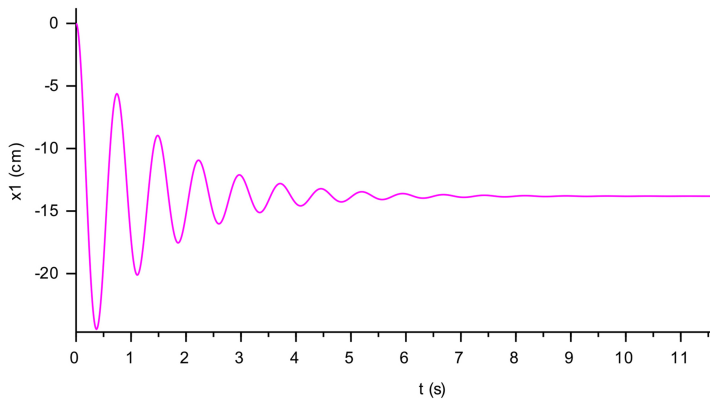
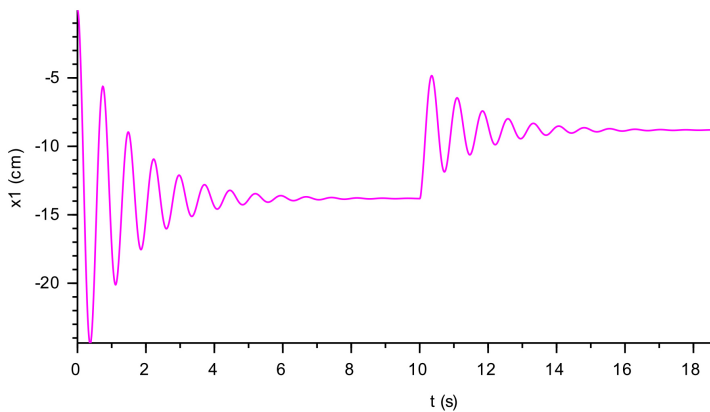*Figure 3.* $w = 0$ *without controller*

Figure 4. $w = 0.05$ *without controller*

reason of the design of the controller, damping force is more effective for the transient phase. Car drivers, travelers, cargoes are more favorable to this situation.
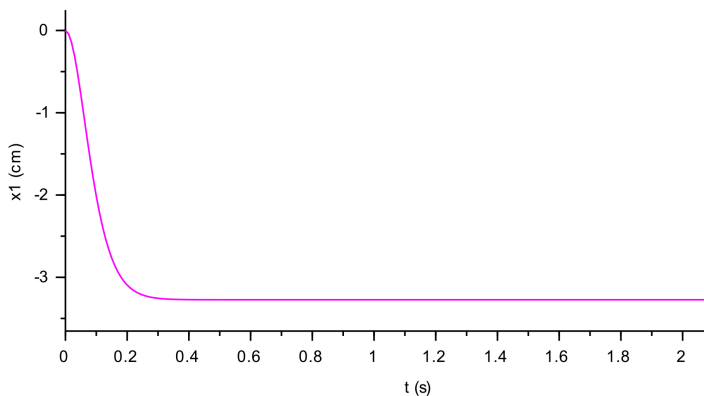

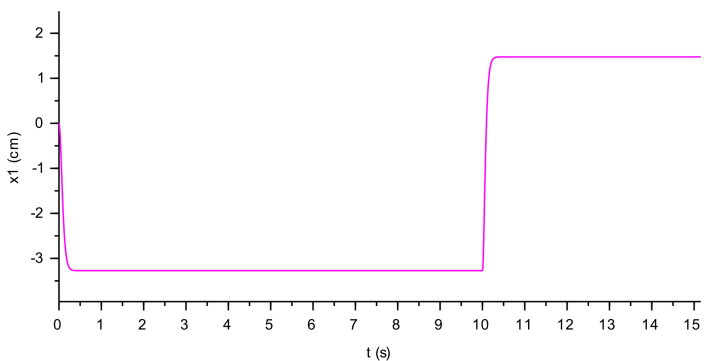*Figure 5.* $w = 0$ *with controller*

Figure 6. $w = 0.05$ *with controller*

The effect of 50 mm road induced displacement is visible (see Fig. 6). Swinging

motions disappear, 10 seconds after reaching the pothole, and after jumping the
stationary state is supervened without swinging. There is state-space equation (22)
without road induced displacement and state feedback (see Fig. 7).
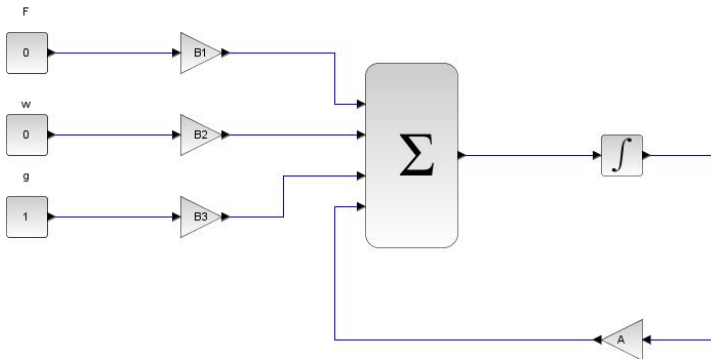
$$\dot{x} = Ax + B_1u + B_2w + B_31 \tag{24}$$
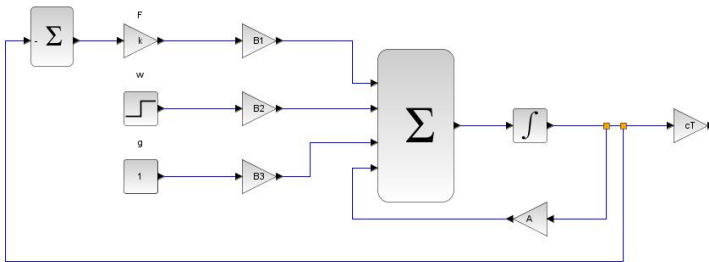

Figure 7. State-space equation model in Xcos

Figure 8. State feedback model in Xcos

The state feedback model is visible, where k is the gain factor (see Fig. 8) The road induced displacement and gravitational acceleration react the system. There isn't reference signal.

4. Conclusion

Designing of the active suspension system of a quarter car model is produced different results besides changing road induced displacement. By the simulation results, the model has much better features with the designed controller. The simulation result of the active suspension system showed that the swinging motion were gone, the stationary state quickly entered, which favored the driver, the passengers, so avoiding cargo damage.

References

[1] A. Hofmann, M. Hanss, Fuzzy arithmetical controller design for active road vehicle suspension in the presence of uncertainties, 2017 22nd International Conference on Methods and Models in Automation and Robotics (MMAR) (2017) pp. 582–587`doi:10.1109/MMAR.2017.8046893`.

[2] L. Bao, S. Chen, S. Yu, Research on active fault-tolerant control on active suspension of vehicle based on fuzzy pid control, Chinese Automation Congress (CAC) (2017) pp. 5911–5916`doi:10.1109/CAC.2017.8243840`.

[3] V. Vidya, M. Dharmana, Model reference based intelligent control of an active suspension system for vehicles, International Conference on circuits Power and Computing Technologies [ICCPCT] (2017) pp. 1–5`doi:10.1109/ICCPCT.2017.8074362`.

[4] L. R. Miller, Tuning passive, semi-active, and fully active suspension systems, Proceedings of the 27th IEEE Conference on Decision and Control (1988) pp. 2047–2053`doi:10.1109/CDC.1988.194694`.

[5] B. Lantos, Control Systems Theory and Design II., 1st Edition, Akadémiai Kiadó, Budapest, 2003.

[6] J. Bokor, P. Gáspár, State-space representation, in: L. Nádai (Ed.), Control Technology with Vehicle Dynamics Applications, 1st Edition, Typotex Elektronikus Kiadó Kft., Budapest, 2008, p. 125.

[7] L. Keviczky, R. Bars, H. J., A. Barta, C. Bányász, Control Engineering, 1st Edition, Universitas-Győr Kht., Győr, 2006.

[8] J. Bokor, P. Gáspár, A. Soumelidis, Control Engineering II., 1st Edition, Typotex Elektronikus Kiadó Kft., Budapest, 2011.

[9] M. Kuczmann, Signals and Systems, 1st Edition, Universitas-Győr Kht., Győr, 2005.

[10] B. Lantos, Control Systems Theory and Design I., 1st Edition, Akadémiai Kiadó, Budapest, 2000.

Characterisation of Diffuse and Local Necking of Aluminium Alloy Sheets Using DIC Technique

Sz. Szalai[1], D. Harangozó[2], I. Czinege[3]

[1]Széchenyi István University, Department of Vehicle Manufacturing
Egyetem tér 1, H-9026 Győr, Hungary
e-mail: szalaisz@sze.hu

[2,3]Széchenyi István University, Department of Materials Science and Technology
Egyetem tér 1, H-9026 Győr, Hungary
e-mail: harangozo.dora@sze.hu, czinege@sze.hu

Abstract: This paper introduces a new method for the characterisation of the boundary of diffuse and local necking based on DIC measurements during tensile tests. A series of images illustrate the extension of diffuse necking and show the occurrence of local necking as well. The evaluation of strain distribution gives the exact description of processes using both time dependent and non-dependent methods.

Keywords: diffuse necking; local necking; tensile test; DIC measurement

1. Introduction

In a uniaxial tension test of aluminium sheets plastic instability and flow localization will occur just after the maximum load and the diffuse necking starts. After the onset of diffuse necking, the deformation continues under the falling load in the form of localized necking, which ultimately leads to ductile fracture.

The necking process was first described by Considère in 1885. According to his well-known criterion, the onset of necking occurs when the hardening rate equals to

the true stress, just when the load reaches its maximum. From that follows that the first derivative of stress by strain equals to the stress:

$$\frac{d\sigma_1}{d\varepsilon_1} = \sigma_1 \qquad (1)$$

Diffuse necking starts from this point and a concentrated strain appears in a specific area of the specimen. The length of this area approximately equals its width. As the deformation continues, local necking occurs which can be characterised by a thin shear band accompanied by a significant decrease in thickness. The onset of local necking can be derived from another instability criterion as equation (2) shows [1].

$$\frac{d\sigma_1}{d\varepsilon_1} = \frac{\sigma_1}{2} \qquad (2)$$

Considering the flow stress curve based on the Hollomon-Ludwik approach $\sigma = K\varepsilon^n$ the onset of diffuse and local necking can be expressed by the n-value using equations (1) and (2). The hardening exponent (n) is defined by the uniform elongation ($A_g\%$) with formula $n=\ln(1+A_g/100)$. The location of diffuse instability according to Hill [2] and other authors [3, 4] is $\varepsilon_D=n$. Similarly, according to equation (2) the true uniaxial strain in tensile direction is $\varepsilon_L=2n$ at the beginning of local necking. The above-mentioned theories were developed originally for mild steels but the $\varepsilon_D=n$ equation is valid for other materials as well [5, 6].

A good summary and further development of necking theory published by Ramaekers [7] with the following basic points:

- Local necking is related to load instability, dF=0.
- It only occurs in a plane strain situation, intensive local thinning before fracture can be characterized by longitudinal and thickness strains.
- During the necking process there is a jump in the strain path from 3 axis to 2 axis strain state.

Taking these points into consideration diffuse and local necking criteria can also be used for evaluating the forming limit diagram (FLD) from Nakazima test results [7].

Newly developed Digital Image Correlation (DIC) techniques are useful tools for the visualization of necking processes, since local deformations of test specimens can be directly observed and strains can be evaluated. Recent publications show that both the PLC bands and post-necking strains can be identified and characterised. Digital image observations are frequently connected to FEM analyses. Coppieters et al [8] introduces an analysis of a model sheet simulating diffuse necking. Similarly,

Kim et al [9] and Tardif et al [10] show DIC images both for diffuse and local necking.

A good comparison of AA5052-O aluminium alloy and DP980 steel can be found in Nguyen et al [11], where DIC images are associated with true strain distribution along the specimen axis. Here it was stated that the localization tendency and localized width of AL5052-O sheet are more significant compared to DP980 sheet. Portlevin-LeChatelier (PLC) bands and intensive shear bands are investigated in Kang et al [12] using AlMg3 samples.

The authors assume that PLC bands play an important role in the development of shear bands before fracture. Because of the very narrow shear band, damage occurs in terms of void nucleation and growth very late in the fracture process, and does not appear to significantly affect tensile ductility. The same observation can be found in Halim et al [13]. However, this latter publication includes that after the onset of local necking, the average strain does not increase in the other parts of the specimen, total strain is concentrated only in the shear band.

The above-mentioned examples are mainly related to tensile tests. Similar necking occurs during Nakazima tests. The main problem of the evaluation of Nakazima tests is how to find the onset of local necking. A possible solution is offered by the ISO 12004-2-2009 standard, where the determination of local necking is derived off-line from the strain distribution before the fracture. This method is called time-independent evaluation. However, there are time-dependent solutions as well, for example Hora et al [14] Merklein et al [15] and Friebe et al [16]. In time-dependent cases a series of strain distributions as the function of time are used for evaluation. Usually time derivatives of longitudinal or thickness strains are applied to mark the onset of local necking and to evaluate the value of minor and major strains.

2. Material and methods

The sheet studied here was AlMg3 (AA5754_H22) alloy with a thickness of 2.5 mm and a chemical composition of 3.41 wt% Mg, 0.18 wt% Mn, 0.17 wt% Si, 0.23 wt% Fe. The width of the tensile specimens was 20 mm, the gauge length was 80 mm and they were cut parallel, 45 degrees and perpendicular to the rolling direction. The tensile tests were carried out with an Instron 5582 machine with strain rate of $2 \cdot 10^{-3}$ 1/s. Local strains were measured during the tensile test with the GOM-ARAMIS® hardware-software system and using the random pattern which has been applied to the specimens previously. Local strains have been determined with GOM-Correlate® software. The diagrams representing the elongation-stress, time-load values and local strains of the specimen were derived from images recorded during the test. GOM-Correlate® software is suitable for determining a wide range of local

strains. In addition to axial, transverse and thickness strains it is also possible to obtain the equivalent (Mises) strain and stress. The strains presented in this study are all defined as equivalent (Mises) strains in percent (%) except for the engineering strains A_g and A_{80}.

3. Results

According to the results of the tensile tests and the digitally recorded time parameter, the information based on images belonging to the elongation can be used to study the onset of diffuse and local necking. Firstly, the material in question was analysed whether it follows equations (1) and (2). To verify the correctness of the formula $\varepsilon_D=n$ and to determine the initiation of diffuse necking, it should be considered which value of the strain hardening exponent is applied to the equation. Engineering strains between 4-6%, 10-15% or 2-(A_g-1)% are considered decisive according to the relevant standard.

Ramaekers [7] also refers to the alteration (initially increasing, then decreasing tendency) of the strain hardening exponent as the function of strain. Figure 1 shows the relation determined from the flow stress curve of a specimen cut parallel to the rolling direction. The horizontal line represents n=0.211 specified by the Hollomon-Ludwik approach, the blue curve shows the values of n numerically calculated from the model of Voce ($k_f=k_{f0}+(k_{f1}+\theta_1\cdot\varepsilon)$ $(1-\exp(\theta_0\cdot\varepsilon/k_{f1}))$) fitted on the flow stress curve, while the triangle indicates the n value measured at the limit of uniform extension from A_g.
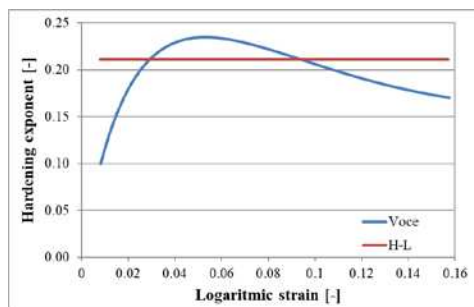

Figure 1. Evaluation of hardening exponent during uniform elongation

As can be seen, the falling section of the strain hardening exponent which is derived from the Voce model, can be approximated with a straight line corresponding to Ramaekers [7]. The whole curve is similar to the functions in Zhemchuzhnikova et al [5]. The location of ε_D-n point reveals that the local value of the strain hardening exponent is approximately 10% higher than ε_D, so $\varepsilon_D=n$ is not

entirely true. At the same time, the strain hardening exponents derived from the Hollomon-Ludwik approach or interpreted between the previously mentioned boundaries (eg. 4-6%), deviate much more from ε_D. Considering that the values of the logarithmic strains at fracture are about 0.2, meeting equation $\varepsilon_D=2n$ is unrealisable. Therefore, another method should be introduced to determine the onset of diffuse and local necking in case of tested aluminium-alloys. The results of DIC technique – to be presented below – can be suitable for this task.

Figure 2 shows a typical image of local strain map with main directions and a section of tensile test diagram of AA574_H22 sheet displaying the necking zone and the time interval to be tested.
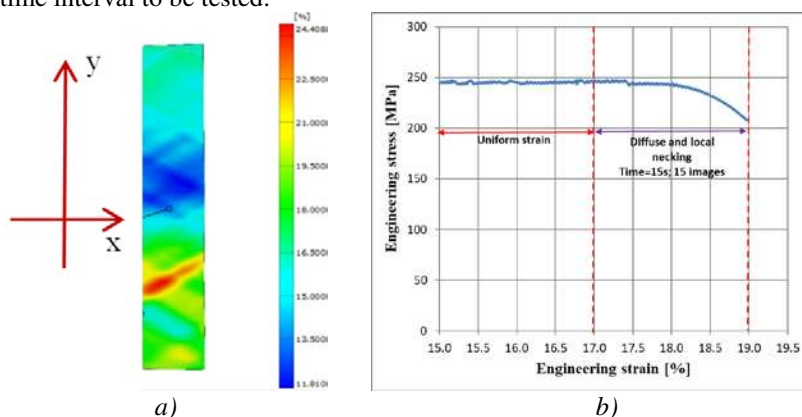

a) *b)*

Figure 2. Illustration of test specimen and diagram
a) local strains and coordinates b) tensile test diagram

Figure 3 shows the map of local strains sampled according to Figure 2 on specimens cut 0-45-90 degrees compared to the rolling direction. The graph under the three different images illustrates the maximum equivalent strain. The first eight pictures of this sequence clearly show the propagation of diffuse necking, while the maximum strain hardly increases in that zone. Therefore, the increment of average strain definitely takes place due to the expansion of the diffuse necking zone. The transition between diffuse and local necking appears in pictures 9-10 when the increase of the maximum strain also starts. The last five pictures clearly show intense localization and a rapid rise in the maximum strain with the appearance of the shear band.

It is interesting that in the recorded sequence of specimen H22_90 two diffuse necking zones appear first, then the lower one vanishes when local necking begins. In the recorded sequence of specimen H22_0 a special phenomenon can be observed

in pictures 12-13, namely a bidirectional intense strain band which aligns to the definite direction related to the fracture in picture 14.
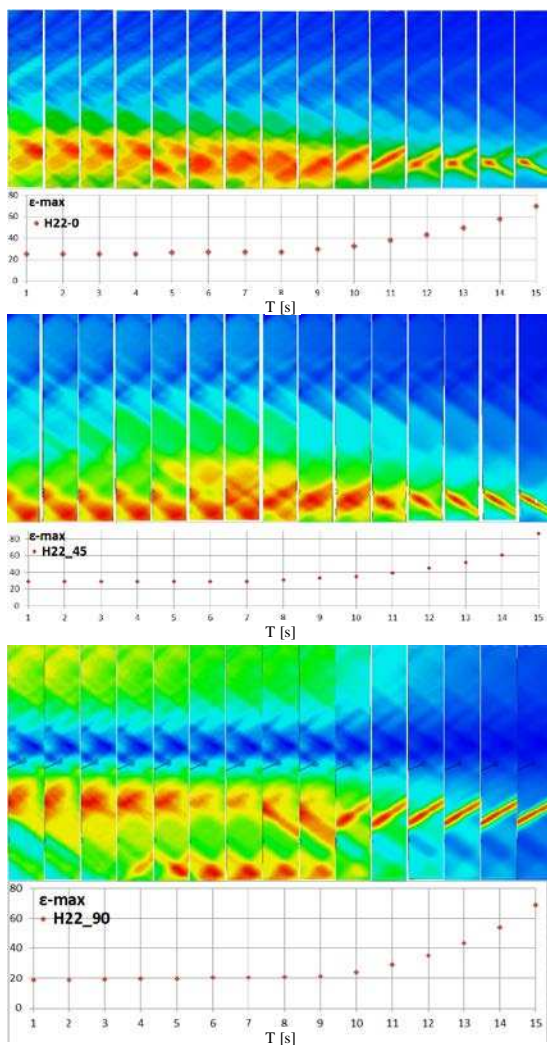

Figure 3. Time history of diffuse and local necking

Shear bands align at an angle of approximately 60° to the axis of the specimen, which deviates from the theoretical 55°. In literature there are also examples of

results approximating 60°. Observing the images together, it can be ascertained that the end of diffuse necking occurs in the ninth picture for all three specimens and local necking starts from the tenth picture. The graphs under the images show that the maximum strain can be a proper parameter to determine the boundary of the two types of necking.
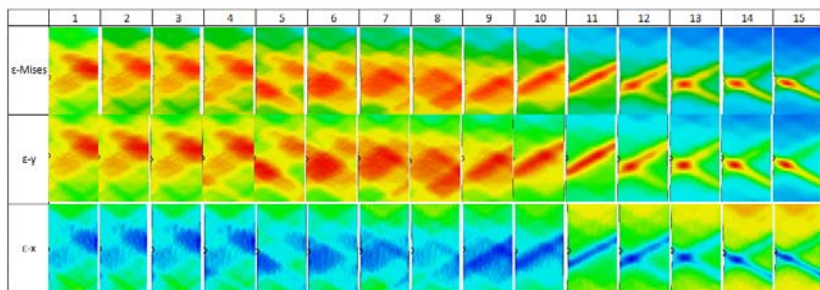

Figure 4. Comparison of Mises (ε-Mises), longitudinal (ε-y) and thickness (ε—x) strains

The equivalent (Mises) strain, the longitudinal (ε-y) and the thickness (ε-x) strain can be seen in Figure 4. The Mises and the longitudinal strain distribution is virtually equal, the distribution of the thickness strain follows the shape of the intense deformation zone.
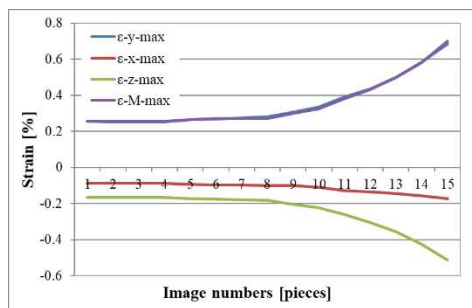

Figure 5. Principal strains and Mises strain vs time

Figure 5 shows strains as the function of time; where the axial strain approximately equals to the equivalent strain, similar to the images in Figure 3. The plot of the thickness (ε-z) strain proves that the thickness reduction is significant in the shear zone which ultimately leads to fracture.
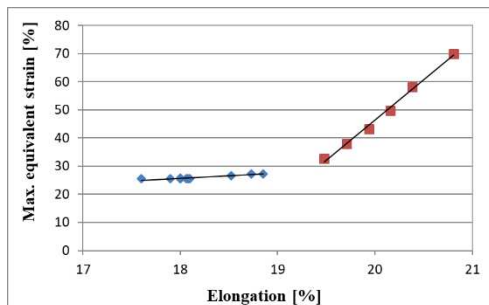
Figure 6. Calculation of the onset of local necking

Figure 6 shows the maximal equivalent (Mises) strain values as the function of the elongation in the area of diffuse and local necking. Eliminating the values of transition between the sections of characteristic diffuse and local necking, linear functions can be fitted for the points. The elongation belonging to the intersection can be specified from the equation of the lines, which is the boundary of diffuse and local necking. Table 1 contains the result of the evaluation completed in all three directions.

Table 1. Calculated and measured strains

| Angle to rolling direction	0°	45°	90°
Uniform strain (A_g [%])	17.8	18.9	15.6
Onset of local necking strain, (ε_L [%])	19.36	21.44	16.35
Tensile strain (A_{80} [%])	20.7	23.2	17.3
Maximum local strain, (ε_{Mmax} [%])	70.0	86.7	69.2
Ratio of onset of local necking strain to uniform strain	0.54	0.59	0.44
Image number at the end of diffuse necking	9	9	9
Image number at the onset of local necking	10	10	10
Mises strain at the onset of local necking, (ε_{Lmax} [%])	32	33	24
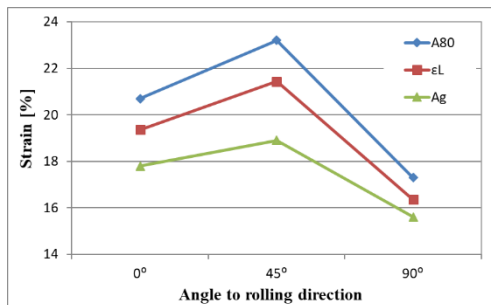
Figure 7. Onset of local necking strain between uniform and tensile strain

Typical measurement points are displayed in Figure 7. The boundary of the diffuse zone is positioned in the middle of the necking zone, similarly to the values in Table 1. The calculated point of intersection and the data from the images are in accordance, since the average strain assigned to the images matches well with the calculated strain. Considering the above points, the maximal strain determin at the onset of local necking (ε_{Lmax}) as shown in the last row of Table 1. The presented method is a time-dependent one, because the boundary of local necking and the major strain is defined based on the images in chronological order and the properties measured in the function of time.
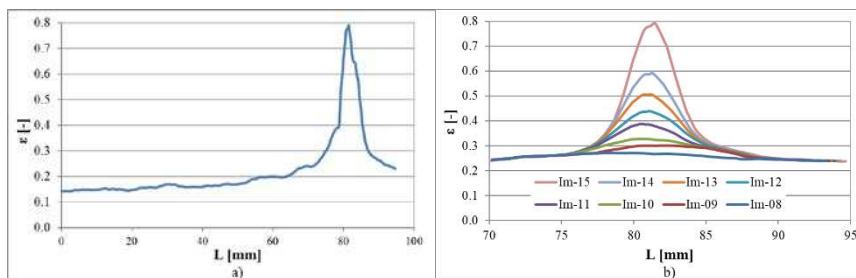

Figure 8. Strain distribution along specimen length
a) strain along total length b) local strains vs length

The information based on the images can be quantified by preparing sections parallel to the axis of the specimen and representing the local strains. Figure 8. a) shows the strain of a 0° specimen on the whole gauge length. In Figure 8. b) strain curves can be seen as the function of time from the area of intensive local necking. Apparently, at the end of diffuse necking, local strain in Im-8 starts to exceed the average strain, but its platform is almost horizontal. Curves of Im-9 and Im-10 show stronger increase, subsequently significant localization starts from image Im-11

which is well illustrated together in the diagram. The same conclusion can be drawn from the images in Figure 3 as from Figure 8, namely local necking appears from Im-9. The value of local necking strain can be specified also from Figure 8 as the maximum of Im-9 curve.

The last image before the fracture (Im-15) provides the opportunity for time-independent evaluation, similarly to the method suggested for the Nakazima-test according to ISO 12004-2-2009. Following the standard, left- and right-side fit windows should be designated to the length-major strain curve. The inner points of the windows are defined by the maximums of the second derivatives of the major strain curve, while the width is provided by an empirical formula. Fitting $f(L)=1/(aL^2+bL+c)$ curve on the measured points, the value of the function at the place of fracture defines the major and minor strain at the start of local necking.

Figure 9 shows the original local strain function, the points of the fitting window and the inverse parabola fitted to the points. The maximum of the fitted function in case of 0° specimen is 0,32 meaning to 32% strain, which equals to the value in the last row of Table 1. Similarly, the results of calculations accomplished in cases of 45° and 90° specimens approach the previously well-specified values. Consequently, both the time-dependent and time-independent methods provided nearly the same result.
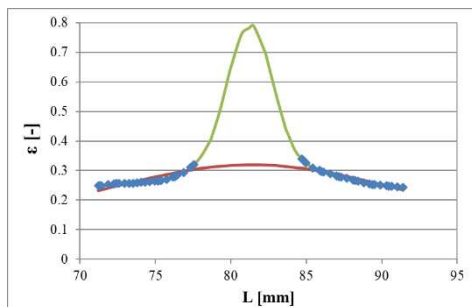

Figure 9. Determination of local necking according to ISO 12004-2-2009 standard

The quantified results of the presented longitudinal sections offer the opportunity to simplify the evaluation and to further characterisa local necking. Studying the shape of the curves, it is apparent that the results of the measurements can be approached with a four-parameter Gaussian function according to equation (3).

$$f(L) = y_0 + A\frac{\sqrt{2/\pi}}{w}e^{-2\left(\frac{L-L_c}{w}\right)^2} \tag{3}$$

In this formula, A stands for amplitude, L_c is the centre of the function, w is the width measured at the points of inflexion and y_o is the vertical offset parameter. Figure 10. a) shows the approaching functions and Figure 10. b) illustrates the first and second derivatives of the Gaussian function. The local coordinates of the maximum of the second derivative providing the inner points of the fitting window, are in a good accordance with the L-coordinates specified by the parabolic approach according to the ISO standard. The calculation of the second derivatives from the Gaussian function is more reliable than from the measured points with significant scattering.
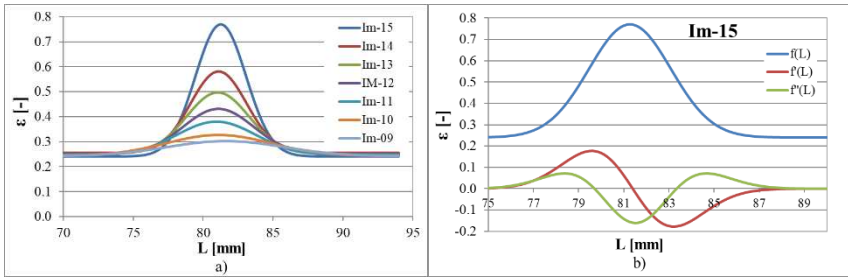

Figure 10. Approximation of local strain with Gaussian function
a) strain distribution maps; b) derivatives of Gaussian function

The time-dependent change of the amplitude coefficients (A=ε_{max}) and the strain belonging to the point of inflexion (ε_l) of the Gaussian functions also shows the increase of these strains. In contrast, the offset parameter (y_o) is roughly constant, so the value of the diffuse strain does not change as the function of time, while a significant increase of local strains appear in the necking band. The distance of inflexion points (w) decrease strongly in the function of time which is a peculiarity of localisation. All these functions can be seen in Figure 11.
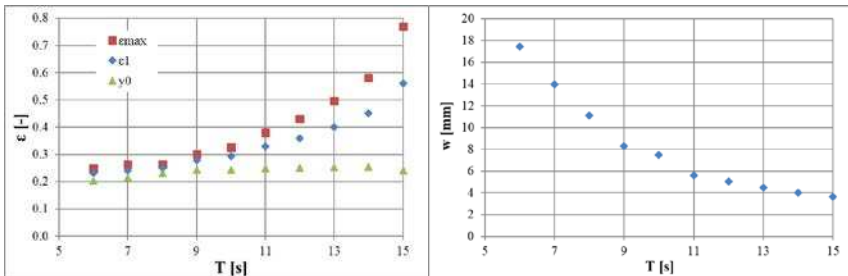

Figure 11. Change of Gaussian parameters versus time

4. Summary and conclusions

The result of the research clearly certifies that the DIC technique is suitable for determining the boundary of diffuse and local necking and the value of the major and minor strain at the onset of local necking during tensile tests.

The boundary of diffuse and local necking can be determined by subjective estimation from the images, which can be precised by specifying the intersection of lines fitted for the points of average and maximal strain. This time-dependent method of evaluation provides reproducible results.

The evaluation can be executed according to ISO 12004-2-2009 from the values of the last strain curve before the fracture. This showed adequate agreement with the time-dependent method. Furthermore, based on the identified regularities, the major and minor strain can be estimated at the boundary of local necking through the results of the tensile tests.

The analysis of strain curves demonstrated that they can be approximated well with four parameter Gaussian functions whose coefficients characterise the necking zone, and they can also provid opportunity to precisely determine the second derivative of the strain.

Acknowledgement

References

[1]   J. G. Sevillano: Plastic anisotropy, formability and strain localisation. TECNUN, Materials Engineering.
URL
http://www4.tecnun.es/asignaturas/estcompmec/documentos/thinsheets.pdf

[2]   R. Hill: On the discontinuous plastic states, with a special reference to localized necking in thin sheets. Journal of the Mechanics and Phisics of Solids 1 (1) (1952) pp. 153-161.
doi: https://doi.org/10.1016/0022-5096(52)90003-3

[3]   J. M. Choung and S. R. Cho: Study on true stress correction from tensile tests. Journal of Mechanical Science and Technology 22 (6) (2008) pp. 1039-1051. doi: https://doi.org/10.1007/s12206-008-0302-3

[4]   A.S. Korhonen, T. Manninen, J. Larkiola: Comparison of forming and fracture limits of cold rolled high-strength austenitic stainless steels. IDDRG 2010, Graz, pp. 535-543.

[5]   D. Zhemchuzhnikova, M. Lebyodkin, D. Yuzbekova, T. Lebedkina, A. Mogucheva, R. Kaibyshev: Interrelation between the Portevin Le-Chatelier effect and necking in AlMg alloys. International Journal of Plasticity November 2018, pp. 95-109. doi: https://doi.org/10.1016/j.ijplas.2018.06.012

[6]   M. Tisza, G. Gál, A. Kiss, P. Z. Kovács, Zs. Lukács: Classic sheet formability tests for qualifying high strength steel sheets. Proceedings of Miskolc University, Multidisciplinary Sciences 4 (1) (2014) pp. 39-48, in Hungarian.

[7]   J.A.H. Ramaekers: A criterion for local necking. Journal of Materials Processing Technology 103 (1) (2000) pp. 165-171. doi: https://doi.org/10.1016/S0924-0136(00)00410-6

[8]   S. Coppieters, J.-H. Kim, K. Denys, S. Cooreman, D. Debruyne: On Complete Solutions for the Problem of Diffuse Necking in Sheet Metal. Procedia Engineering 207 (2017) pp. 2012–2017. doi: https://doi.org/10.1016/j.proeng.2017.10.1060

[9]   J.-H. Kim, A. Serpantié, F. Barlat, F. Pierron, M.-G. Lee: Characterization of the post-necking strain hardening behavior using the virtual fields method. International Journal of Solids and Structures 50 (24) (2013) pp. 3829–3842. doi: https://doi.org/10.1016/j.ijsolstr.2013.07.018

[10] N. Tardif, S. Kyriakides: Determination of anisotropy and material hardening for aluminum sheet metal. International Journal of Solids and Structures 49 (2012) pp. 3496–3506. doi: https://doi.org/10.1016/j.ijsolstr.2012.01.011

[11] V-T. Nguyen, S-J. Kwon, O-H. Kwon and Y-S. Kim: Mechanical Properties Identification of Sheet Metals by 2D-Digital Image Correlation Method. Procedia Engineering 184 (2017) pp. 381–389. doi: https://doi.org/10.1016/j.proeng.2017.04.108

[12] J. Kang, D.S. Wilkinson, M. Jain, J.D. Embury, A.J. Beaudoin, S. Kim, R. Mishira, A.K. Sachdev: On the sequence of inhomogeneous deformation processes occurring during tensile deformation of strip cast AA5754. Acta Materialia 54 (2006) pp. 209–218.
doi: https://doi.org/10.1016/j.actamat.2005.08.045

[13] H. Halim, D. S. Wilkinson, M. Niewczas: The Portevin–Le Chatelier (PLC) effect and shear band formation in an AA5754 alloy. Acta Materialia 55 (2007) pp. 4151–4160.

[14] P. Hora, B. Berisha, M. Gorji, N. Manopulo: A generalized approach for the prediction of necking and rupture phenomena in the sheet metal forming. IDDRG Conference 2012, Mumbai, India.
URL https://www.researchgate.net/publication/269709664

[15] M. Merklein, A. Kuppert, M. Geiger: Time dependent determination of forming limit diagrams. CIRP Annals - Manufacturing Technology 59 (1) (2010) pp. 295–298.
doi: https://doi.org/10.1016/j.cirp.2010.03.001

[16] H. Friebe, T. Möller: Aktueller Stand der zeitabhängigen Verfahren. Presentation des Arbeitskreises NAKAJIMA, Stand 28.02.2012, Düsseldorf. GOM documenation.
URL https://www.gom.com/

Sensitivity Study of a Nonlinear Semi-Active Suspension System

F. Hajdu

Széchenyi István University, Faculty of Mechanical Engineering, Informatics and Electrical Engineering, Department of Mechatronics and Machine Design
Egyetem tér 1., 9026 Győr, Hungary
e-mail: hajdfl@sze.hu

Abstract: In this paper the OAT (one-at-a-time) sensitivity analysis of a nonlinear semi-active suspension system is carried out with numerical simulation. A specific property of the system is chosen for measure sensitivity, which can be calculated with numerical simulations easily. Both the sensitivity of the system and the input parameters were examined. The degree of sensitivity was measured with a sensitivity index and based on it sensitivity Fuzzy-sets were established. A simple method to reduce sensitivity of a certain parameter is also proposed.

Keywords: sensitivity analysis, numerical simulation, nonlinear system modelling

1. Introduction

Parameter sensitivity analysis is used in several fields of engineering and science. It is used to find out how the change in parameters affect the systems behaviour [1]. Parameter identification [2] and inverse simulation [3] tasks can also be solved with sensitivity study. From sensitivity, the uncertainty of a system can also be calculated [4]-[5].

In this paper, the local or One-at-a-time (OAT) parameter sensitivity study of a Duffing-type semi-active suspension system is carried out. The aim of this research is to test a simple method to find out which parameters influence the system's behaviour the most and to develop an easy, fast methodology, which can be used in case of more complex systems as well. A specific property of the system is chosen for measure sensitivity, which can be calculated with numerical simulations easily. The presented results can be used later for control tasks.

The paper is organised as follows: after a short literature review the sensitivity analysis with RMS (root mean square) of the acceleration is described, then the examined nonlinear Duffing-type semi-active suspension system is presented shortly. In the next section, the sensitivity analysis of the system and the input parameters is described in detail and a simple method is also proposed to reduce sensitivity.

2. Parameter sensitivity analysis

To obtain the sensitivity of a nonlinear system there are several methods ranging from partial differentiation techniques to statistical tests. A detailed review of the most common methods can be found in [6]. As the methods and their applicability are different in this paper only some engineering examples of local sensitivity analysis are presented. A more detailed review of sensitivity study methods and engineering applications is planned in another paper.

Local sensitivity analysis is widely used in environmental engineering tasks. The aim of the study presented in [7] is to identify the most influencing constant parameters of Two-Source Energy Balance Model over an irrigated olive orchard in semi-arid areas with OAT sensitivity study. In [8] OAT sensitivity analysis using Sequential Uncertainty Fitting algorithms was performed to examine the critical input variables of the study area in case of a soil and water assessment tool model for the Langat River basin, Malaysia to predict stream flows. A similar study is presented in [9], where the OAT sensitivity analysis of 13 parameters was carried out to examine the applicability of the SWAT model in the Gumera river basin upstream of Lake Tana, Ethiopia for simulating stream runoff and sediment load. In [10] the local sensitivity analysis of a thermal model of the ZEB Test Cells Laboratory was carried out in terms of temperature profiles of the internal air and internal surfaces with 49 parameters. Based on the local sensitivity analysis and on in-field observations, some actions were suggested to improve the accuracy of the predictions of the thermal behaviour of the test cell.

Local sensitivity studies can be applied in other engineering fields too. In [11] the local sensitivity analysis of a hydraulic servo and a conceptual landing gear model of the Gripen aircraft with Effective Influence Matrix and the Main Sensitivity Index is presented.

Local sensitivity analysis can be effectively used in medical sciences too. It was used for example to find sensitive parameters and their confidence intervals in order to estimate cardiovascular network parameters in the case of the arm arteries [12].

From the literature study, it can be concluded, that OAT sensitivity analysis can be used effectively both in engineering and other sciences as well in order to examine

the effects of different parameters on the system's behaviour. In this study, an OAT sensitivity study is carried out to examine the effects of parameter changes in the case of a semi-active suspension system.

2.1. Sensitivity analysis of the suspension system

In the case of vibration analysis, the RMS (root mean square) of the acceleration is widely used [13]. It reflects the energy content of the vibration. The RMS of the acceleration can be calculated with the following formula [14]:

$$RMS = \sqrt{\frac{\sum_{i=1}^{n} a_i^2}{n}} \tag{1}$$

where a_i is the acceleration value at a time interval and n is the number of acceleration values.

The method for calculation of the RMS in numerical simulation can be seen in Fig. 1.
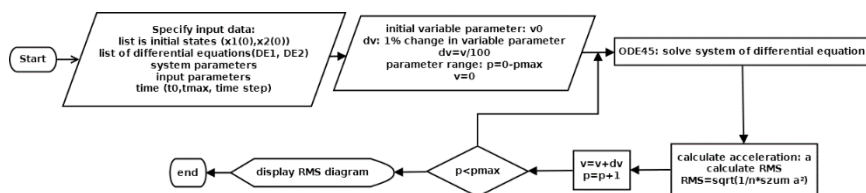

Figure 1. Calculating the sensitivity diagram

It was examined how 1% change in the selected parameter changes the RMS value. The parameter range was 0-300%. The parameter is considered sensitive when a small change (1%) in a parameter changes the RMS value rapidly (slope of the RMS curve). Sensitivity is expressed with Sensitivity Index (SI), which can be calculated as the ratio between the relative change in RMS and the relative change in the selected parameter [9]:

$$SI = \frac{\text{change in RMS } [\%]}{\text{change in parameter } [1\%]} \tag{2}$$

Based on initial simulation results the following Fuzzy sets [15]-[16] are determined depending on the Sensitivity Index to reflect the degree of sensitivity.

1. not sensitive: SI<=0.1

2. moderately sensitive: 0.1<SI<=0.6

3. sensitive: 0.6<SI<2

4. extremely sensitive: 2<SI

In the next sections, the parameter sensitivity analysis of a semi-active suspension system is examined. With the specified Fuzzy-sets it determined how sensitive the system parameters and the input parameters are.

3. Semi-active suspension system model

In this study, a semi-active suspension system with magneto-rheological damper is examined with a quarter car model (Fig. 2). This model was previously studied with bifurcation and phase-plane diagrams. It was observed that in extreme cases chaotic oscillation can occur [17].
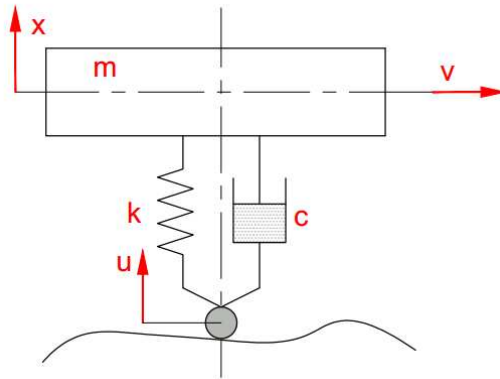

Figure 2. Semi-active suspension system model

It is assumed, that the spring has a Duffing type nonlinear restoring force described by the following equation:

$$F_s = -\beta x - \alpha x^3 \tag{3}$$

The damping is assumed to be a variable constant. The road profile was assumed to be sinusoidal, which is the model of an undulated road [19].

The equation describing the system's behaviour is:

$$\frac{d^2}{dt^2}x(t) + \frac{k}{m}\frac{d}{dt}x(t) + \frac{c}{m}(-x(t) + 1000x(t)^3)x(t) = A\sin\left(\frac{2\pi v}{\lambda}t\right) \tag{4}$$

where m is the mass of the vehicle; k is the damping coefficient, c is the stiffness of the spring, A is the amplitude of the road, v is the vehicle speed and λ is the wavelength of the road. The initial parameters were based on [18] and are shown in Table 1.

Table 1. Initial simulation parameters

Parameter	Name	Value	Unit
m	mass of vehicle	375	kg
k	spring stiffness	35000	N/m
c	damping coefficient	100	Ns/m
v	vehicle speed	50	km/h
A	amplitude of road	0.1	m
λ	wavelength of road	10	m

Numerical simulations were carried out with Maple. *ODE45* numerical solver was used with 0.01 step size and the maximum time was 50 s.

4. Sensitivity study of the suspension system

In this section, the sensitivity analysis of the semi-active suspension system is presented. First, the parameters of the suspension, like the mass of the vehicle, the spring stiffness, and the damping coefficient were examined which is followed by the input parameters like the speed of the vehicle and the wavelength and the amplitude of the road. Then a simple method for reducing the sensitivity of an input parameter is proposed.

4.1. System parameters

In Fig. 3, the sensitivity of the mass of the vehicle can be seen. When *400 kg<m<600 kg* it is not sensitive. When *500 kg<m<810* kg there is a rapid change in the RMS. *SI=0.42*, therefore this parameter is moderately sensitive. The highest RMS value is at 810 kg, after that it decreases linearly. The RMS value is the lowest when *m=500* kg. If the other parameters won't change it is advised to enlarge the mass of the vehicle to 400 kg.
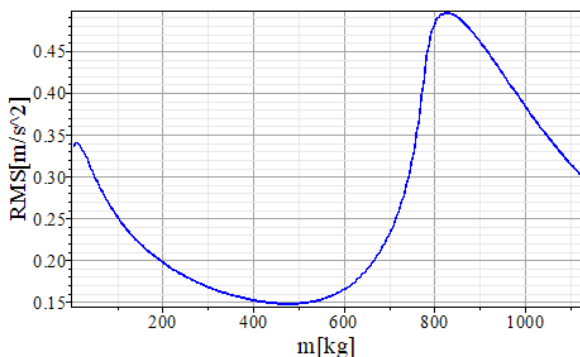
Figure 3. Sensitivity of the mass

In Fig. 4, the sensitivity of the damping coefficient can be seen. When the damping coefficient is low ($c < 100$ *Ns/m*) it is extremely sensitive, *SI=9*. When $c = 0$ chaotic oscillation can also occur [17]. When *100 Ns/m < c < 500 Ns/m SI=0.875*, therefore it is sensitive. When $c > 1000$ Ns/m it is not sensitive. It is a good result, as this parameter can be changed, therefore it can be used for control tasks.
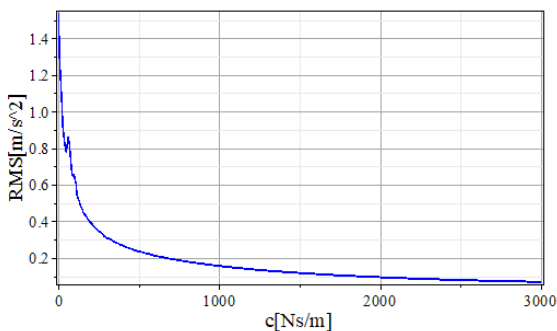

Figure 4. Sensitivity of the damping coefficient

In Fig. 5 the sensitivity of the spring stiffness can be seen. It changes the RMS almost linearly, it is not linear only, when it is low ($k < 15000$ *N/m*), in that case, the parameter is moderately sensitive with *SI=0.53*. When $k > 15000$ *SI=0.175*, which means this parameter is moderately sensitive in this range too.
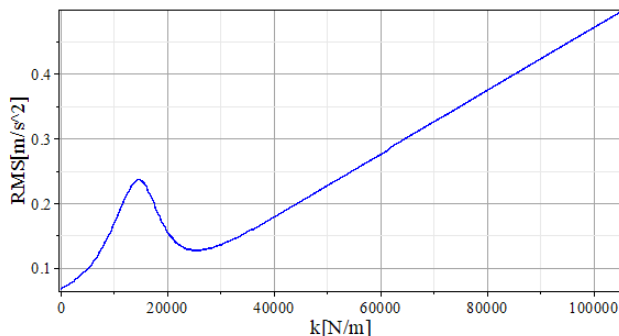
Figure 5. Sensitivity of the spring stiffness

4.2. Input parameters

In Fig.6 the sensitivity of the vehicle speed can be seen. When *v<60 km/h* or *v>110 km/h* it is not sensitive. When *60<v<95* km/h there is a rapid change in the RMS. The highest RMS value is at 77 km/h, therefore it is the most hazardous speed on this road. *SI=0.66* when *60 km/h<v<77 km/h*, and *SI=0.486* when *77km/h<v<95 km/h*. This is an important observation as the speed of the vehicle can be easily changed. The sensitive speed range is the case of travelling on a carriageway with a speed limit of 90 km/h.
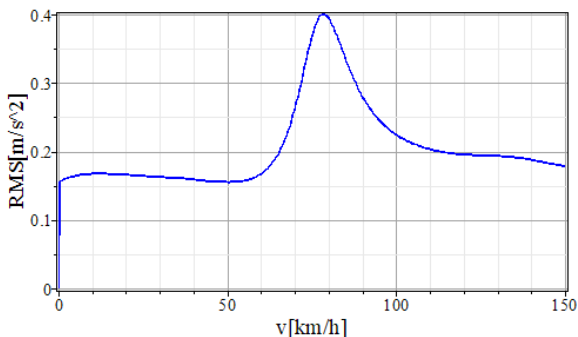

Figure 6. Sensitivity of the vehicle speed

In Fig. 7 the sensitivity of the amplitude of the road can be seen. This parameter is not sensitive as the maximum value of *SI=0.03*. The RMS increases linearly as A is increased if *A>0.1* m.
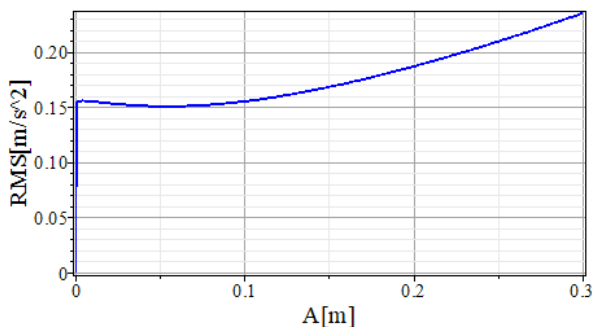
Figure 7. Sensitivity of the amplitude of the road

In Fig. 8 the sensitivity of the wavelength of the road can be seen. When $\lambda<3$ *m* or $\lambda>9$ *m* it is not sensitive. When *4 m<λ<6 m* SI=1.025 and when *6<λ<9 SI=0.83*. The wavelength of the road can vary rapidly because of road failures [20], therefore this is the parameter, which should be given particular attention.
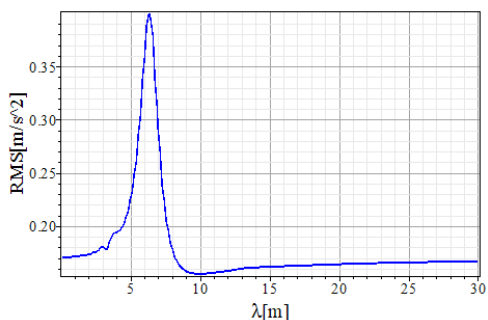
Figure 8. Sensitivity of wavelength of the road

4.3. Sensitivity of parameters

The results are summarized in Table 2. From the system parameters, the damping coefficient is the most sensitive. It is extremely sensitive when it is of low value. This is the parameter, which can be used for the control task as it can be adjusted. It must be ensured that it should not be reduced below 500 Ns/m and that damper failure not to occur. The mass of the vehicle and the spring stiffness are moderately sensitive and the amplitude of the road is not sensitive. The speed of the vehicle and the wavelength of the road are sensitive. From them, the speed of the vehicle can be controlled. The wavelength of the road can change rapidly and cannot be controlled, therefore its effects are further analysed in the next Session.

Table 1. Sensitivity of parameters

Parameter	SI_{max}	Sensitivity (Fuzzy-set)
m	0.42	2
c	9	4
k	0.53	2
v	0.66	3
A	0.03	1
λ	1.25	3

4.4. Reducing sensitivity with adjustable damping coefficient

In this section, it is examined how the sensitivity of the wavelength can be reduced by changing the damping coefficient. The simple case is to enlarge the damping coefficient to until 3000 Ns/m. Another option is to vary the damping coefficient and enlarge it only, where the sensitivity is large and reduce it when it is low. An example of an adjustable damping coefficient can be seen in Fig. 9.
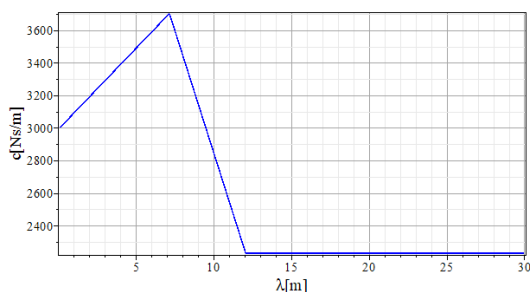
Figure 9. Adjustable damping coefficient based on the wavelength of the road

In Fig. 10 the simulation results are shown. It can be seen that with a larger value of damping coefficient not only the sensitivity to the wavelength can be reduced, but the overall value of the RMS too. *SI=0.175* in case of constant *c=3000 Ns/m* and *SI=0.125* in case of adjustable damping coefficient, therefore this parameter becomes moderately sensitive instead of sensitive. It can be concluded that the sensitivity of a parameter can be reduced by changing another parameter. This observation can be important in the case of controller design later on [21].

Figure 10. Sensitivity of the wavelength with different damping coefficients (blue: c=1000, black: c=3000, red: adjustable)

5. Conclusions and further research tasks

In this paper, the OAT sensitivity analysis of a nonlinear semi-active suspension system was carried out with numerical simulations. Fuzzy-sets were established to measure the degree of sensitivity. It was observed that from the system parameters the damping coefficient is the most sensitive, but onl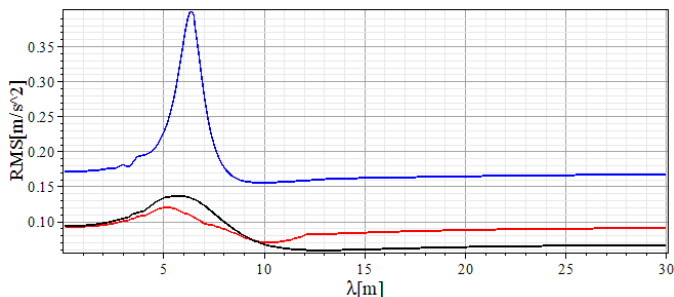y when its value is small. From the input parameters, the wavelength of the road is the most sensitive, which can be reduced by changing the damping coefficient. This observation can be the basis of control tasks later. The main task of further research is to examine the effectiveness of the presented method to measure sensitivity and to use it on other examples, like a fire truck suspension system or measured road failures. Later the global sensitivity analysis of the system will be also carried out to acquire more comprehensive knowledge about the behaviour of systems. Another important task is to speed up with parallelization [22]-[24] and to further develop the method in a way to be effectively used in control theory tasks. A long term task is to utilize an optimization algorithm to adjust the parameters to gain an optimal solution in order to reduce the sensitivity of the system.

Acknowledgement

References

[1] S. Farahat, H. Ajam, Sensitivity Analysis of Parameter Changes in Nonlinear Hydraulic Control Systems, International Journal of Engineering, Transactions B: Applications. 18 (3) (2005), pp. 239-252

[2] J. Iwaniec, Sensitivity Analysis of an Identification Method Dedicated to Nonlinear Systems Working Under Operational Loads, Journal of Theorethical and Applied Mechanics. 49. (2011) pp. 419-438.

[3] D. J. Murray-Smith, The Application of Parameter Sensitivity Analysis Methods to Inverse Simulation Models, Mathematical and Computer Modelling of Dynamical Systems 19 (1) (2012), pp. 1-24. doi: 10.1080/13873954.2012.696271

[4] J. Zádor, I. Gy. Zsély, T. Turányi, M. Ratto, S. Tarantola, A. Saltelli, Local and Global Uncertainty Analyses of a Methane Flame Model, J. Phys. Chem. A 109 (43) (2005), pp. 9795-9807. doi: 10.1021/jp053270i

[5] T. Turányi, Local sensitivity analysis, lecture notes, COST CM1404 Training School on the analysis, uncertainty quantification, validation, optimization and reduction of detailed combustion mechanisms for practical use of smart energy carriers, Eötvös Lóránt University, [cited 2019.03.23], URL: http://garfield.chem.elte.hu/COST_Training_School_2016/overheads/Turanyi _1-2_Local_Sensitivity_Analysis.pdf

[6] D. M. Hamby, A Review of Techniques for Parameter Sensitivity Analysis of Environmental Models, Environmental Monitoring and Assessment 32 (2) (1994), pp. 135-154. doi: 10.1007/BF00547132

[7] A. Mouida1, N. Alaa, Sensitivity Analysis of TSEB Model by One-Factor-At-A-Time in Irrigated Olive Orchard, International Journal of Computer Sciences Issues. 8 (3). (2011) pp. 369-377.

[8]   K. Khalid, M. F. Ali, N. F. Abd Rahman, M. R. Mispan, Application on One-at-a-Time Sensitivity Analysis of Semi-Distributed Hydrological Model in Tropical Watershed, International Journal of Engineering and Technology 8 (2) (2016), pp. 132-136., doi: 10.7763/IJET.2016.V8.872

[9]   K. H. M. Mamo, M. K. Jain, Runoff and Sediment Modeling Using SWAT in Gumera Catchment, Ethiopia, Open Journal of Modern Hydrology 3 (4), (2013), pp. 196-205. doi: 10.4236/ojmh.2013.34024

[10] G. Cattarin, L. Pagliano, F. Causone1, A. Kindinis, F. Goia, S.Carlucci, C. Schlemminger, Empirical validation and local sensitivity analysis of a lumped-parameter thermal model of an outdoor test cell, Building and Environment 130 (2018), pp. 151-161, doi: 10.1016/j.buildenv.2017.12.029

[11] Y. Jung, Local Sensitivity Analysis of Nonlinear Models – Applied to Aircraft Vehicle Systems, Msc. thesis, Linköping University (2009)

[12] R. Gul, S. Bernhard, Local sensitivity analysis of cardiovascular system parameters, Modelling in Medicine and Biology X 17 (2013), pp. 155-167., doi: 10.2495/BIO130141

[13] Brüel & Krajer: Measuring vibration, [cited 2019.03.01], URL:https://www.bksv.com/media/doc/br0094.pdf

[14] M. Arraigada, M. Partl, Calculation of displacements of measured accelerations, analysis of two accelerometers and application in road engineering, 6th Swiss Transport Research Conference (STRC 2006), Monte Verità, Ascona, Switzerland, [cited 2019.03.15], URL:https://www.dora.lib4ri.ch/empa/islandora/object/empa:8307

[15] P. Baranyi, L.T. Koczy, T.D. Gedeon, A Generalized Concept for Fuzzy Rule Interpolation, IEEE Transactions on Fuzzy Systems 12 (6) (2004), pp. 820-837. doi: 10.1109/TFUZZ.2004.836085

[16] L.T. Kóczy, D. Tikk, Fuzzy Systems (in Hungarian), Typotex kiadó, 2012

[17] F. Hajdu, Numerical Examination of Nonlinear Oscillators, Pollack Periodica: An International Journal for Engineering and Information Sciences 13 (3) (2018), pp. 95-106., doi: 10.1556/606.2018.13.3.10

[18] J. Fakhraei, H.M. Khanlo, M. Ghayour, Chaotic behaviors of a ground vehicle oscillating system with passengers, Scientia Iranica, 24 (3) (2017), pp. 1051–1068. doi: 10.24200/sci.2017.4088

[19] J.C. Dixon, Suspension Geometry and Computation, John Wiley & Sons Ltd., 2009, doi: 10.1002/9780470682906

[20] A.V. Mann, K.J. McManus, J.C. Holden, Power Spectral Density Analysis of Road Profiles for Road Defect Assessment, Road and Transport Research 6 (3) (1998), pp. 36-47.

[21] M. Kuczmann, Comprehensive Survey of PID Controller Design for the Inverted Pendulum, Acta Technica Jaurinensis, 12 (1) (2019), pp. pp. 55-81. doi: 10.14513/actatechjaur.v12.n1.492

[22] F. Hajdu, Gy. Molnárka, Parallel Numerical Creation of Phase-space Diagrams of Nonlinear Systems Using Maple Acta Technica Jaurinensis, 11 (3) (2018), pp. 132-149. doi: 10.14513/actatechjaur.v11.n3.457

[23] F. Hajdu ; Gy, Molnárka Parallelization of Numerical Examination of Nonlinear Systems using Maple In: P, Iványi; B H, V Topping; G, Várady (eds.) Proceedings of the Fifth International Conference on Parallel, Distributed, Grid and Cloud Computing for Engineering, Civil-Comp Press, (2017) Paper 30, doi: 10.4203/ccp.111.30

[24] F. Hajdu, Parallel Numerical Creation of 2-parametric Bifurcation Diagram of Nonlinear Oscillators, Acta Technica Jaurinensis, 11 (2) (2018) pp. 61-83. doi: 10.14513/actatechjaur.v11.n2.453

Review of Finite Element Vehicle Interior Acoustic Simulations Including Porous Materials

J. Kun[1], D. Feszty[2]

**Department of Whole Vehicle Development, Audi Hungaria Faculty of
Automotive Engineering, Széchenyi István University,
Egyetem tér 1., 9026 Győr, Hungary
[1]e-mail: kun.janos@ga.sze.hu
[2]e-mail: feszty.daniel@sze.hu**

Abstract: Recent trends in vehicle engineering require manufacturers to develop
             products with highly refined noise, vibration and harshness levels. The
             use of trim elements, which can be described as Poroelastic Materials
             (PEM), are key to achieve quiet interiors. Finite Element Methods
             (FEM) provide established solutions to simple acoustic problems.
             However, the inclusion of poroelastic materials, especially at higher
             frequencies, proves to be challenging. The goal of this paper was to
             summarize the state-of-the-art as well as to identify the challenges in
             the acoustic simulations involving FEM-PEM methods. This involves
             investigation of measurement and simulation campaigns both on
             industrial and fundamental academic research levels.

Keywords: finite element method, poroelastic materials, vehicle acoustics

1. Introduction

Continuous development in the automotive industry has led customers to expect
quieter and more efficient vehicles for their daily commute. Megatrends, such as the
need to reduce the environmental footprint of vehicles, urbanisation or the general
increase in the need for mobility have shifted paradigms for vehicle producers.
Buyers today prefer intelligent, efficient and comfortable cars instead of vehicles
requiring the increased level of driver control or exposure to tiring noises, vibrations

as well as harsh, intrusive effects in the cabin. As a result of the aforementioned effects, today's mainstream vehicles require engineering sophistication that was formerly typical for luxury cars only. This manifests itself in the need for accurate engineering methods to achieve the desired vehicle characteristics, rather than just the usage of fine materials. To satisfy customers, highly scientific methods have to be applied during the design process of cars. Today, the noise, vibration and harshness (NVH) level is one of the key vehicle properties customers care of. This does not necessarily mean quite vehicles in every case. While mainstream vehicle models are expected to be quieter and smoother, their performance oriented versions need to have a unique sound character to them, to provide an aural excitement beside driving enjoyment. Both of these development targets mean that achieving the desired acoustic characteristics has gained huge importance within the vehicle development process.

The advent of the electric car places even more focus on acoustics. Electric powertrains are on one hand quieter than internal combustion engines, while on the other hand will excite the vehicle chassis at much higher frequencies, than their traditional counterparts. This means that acoustic treatments are expected to perform well not only at low frequencies (where chassis noises "masked" earlier by the combustion powertrain will now be audible) as well as high frequencies, where the excitation from e-motors will dominate [1]. Alongside the improved acoustic performance, however, stricter efficiency goals will dictate continuous weight savings as well. Both of the above mentioned, conflicting requirements coupled with the accelerated development cycles necessitate accurate numerical methods to determine acoustic properties in the early phases of the design process.

The goal of the present paper is to provide a comprehensive overview in recent developments of simulating vehicle interior acoustics via FEM-PEM methods. The paper can aid researchers in understanding the state-of-the-art of vehicle interior acoustic simulations as well as the challenges of this field, thus leading to the identification of the gaps in knowledge.

2. Theoretical background of FEM-PEM simulations

2.1. Acoustic excitation modes in vehicle acoustics

Road vehicles are subjected to a wide range of mechanical and acoustic excitations.

Fundamentally, passengers hear noises through the pressure waves transmitted to their ear drums in the air in the cabin compartment. However, these pressure waves can be induced in two fundamentally different ways, which is the classical distinction between noise sources in a vehicle [2]:

- Structure-borne noise: Noise induced by the physical impact of an object on a structure and this signal travelling within the structure. For vehicles, this would correspond to time varying loads (i.e. vibrations) entering the vehicle chassis from the road and tyres, or elements of the powertrain. An example can be the vibratory load entering the chassis through the tyres, rims and suspension due to uneven road, or the vibrations entering the chassis from the engine vibrations. Typical frequency range is between 20-400 Hz

- Airborne noise: Noise induced by aerodynamic loads or the acoustic radiation of an object and entering the structure of interest via air. For vehicles, this corresponds to time-varying loads (i.e. vibrations) entering the vehicle chassis through the air around the vehicle. Examples are the vibration of the roof due to turbulent flow around it, the pressure waves radiated by the engine in the engine bay, or the tyre surfaces as the tyre is periodically deformed at the tyre-road interface Typical frequency range is 500 Hz and above.

These two noise categories are distinctively important in the literature review, since many software applications are restricted to the prediction of one or the other only. Fig. 1 illustrates the typical frequency ranges and sources of structure-borne and airborne noise for vehicles.
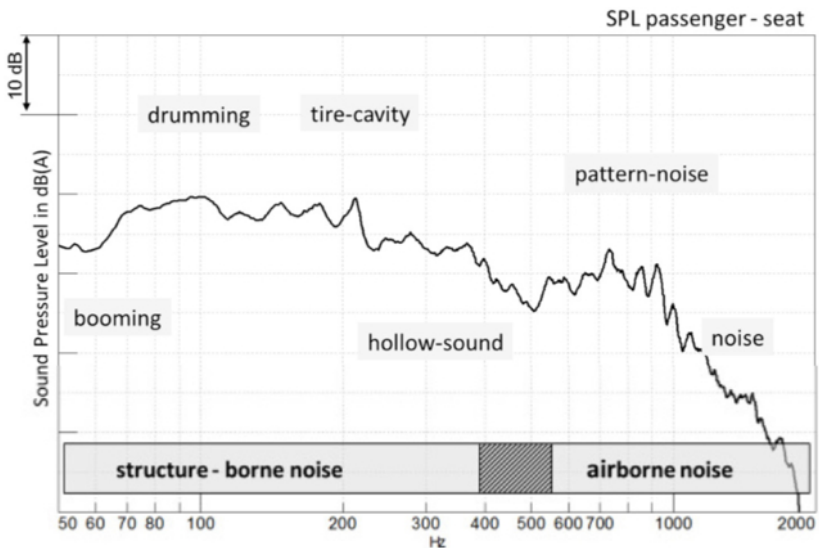

Figure 1.: Frequency range of structure-borne and airborne noise components [2]

Both noise sources lead to the vibration of the chassis elements (such as body panels, windshields, trim elements, etc.) and this vibrational energy transforms to pressure waves inside the passenger compartment, which then excite the eardrum of the passengers.

2.2. Finite Element Method

Finite Element Methods (FEM) can be used not only for stress and strength analysis, but also for predicting the acoustic behaviour of a structure. Structural problems are solved using a stiffness matrix as well as a displacement- and a load vector, while in acoustic dynamic analyses these are supplemented by mass/ and damping matrices, as well as acceleration and velocity vectors. Detailed description of structural FEM can be found in [3] and [4], while the acoustic coupling theory is expanded in [5] and [6].

For acoustic simulations, it is necessary to model the air surrounding the vibrating solid object. To determine the pressure field in air, coupled solutions are used where the stiffness matrix contains the coupling between the structure and air cavity. Song et al. [7] and Kim and colleagues [8] worked extensively on developing acoustic coupling formulations. For solving these equations, multiple solution schemes exist, with substructuring and modal analysis being the two most predominant ones in the industry.

2.3. Poroelastic Material (PEM) modelling

A recent addition to the Finite Element Method simulations has been the modeling of Poroelastic Materials (PEM). Poroelastic materials consist of a structural, porous matrix whose cavities can be filled with various fluids [9]. Figure 2. illustrates a sample cross-section of a poroelastic material. For automotive applications, poroelastic materials form for example the trim panels in the interior, carpets, seats and in general, i.e. most of the sound-absorption materials applied. Therefore, although their structure may differ, the fluid phase is always air. Interaction between these distinct phases complicates material behaviour in case of an excitation. As cavity diameters are on the microscale, computational capacity of current computers prevents the direct modelling of these structures, as cell numbers in a Finite Element solver would be excessive. To account for their effect, they can simply be modelled as non-structural masses added to the load-carrying structure [21, 22, 23, 24] or by applying the so-called Biot-theory for modelling PEM materials. Biot-theory describes the behaviour of PEM materials using about 13 macroscopic parameters (the number depends on the equation formulation) [10, 11, 12, 13], which are extracted from measurements. Since most of the Biot-parameters are both material- and frequency-dependent, their accurate measurement and application in numerical

campaigns poses considerable challenges [14, 15, 16, 17]. However, the use of the Biot-theory in FEM simulations improves the comparison between experiments and numerical simulations greatly, especially when compared to the non-structural mass approach. FEM-PEM results match the experiments to higher frequencies, which justifies the extra computational cost imposed.
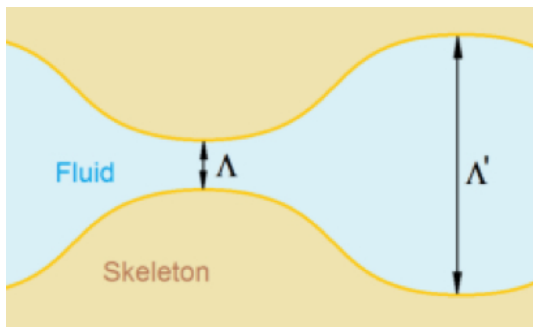

Figure 2.: cross-section of a generic poroelastic material [9]

The following sections will summarize selected works from the topic of FEM-PEM simulations, to highlight the state-of-the-art in this field and to point out certain gaps in the knowledge in this field.

3. Review of relevant literature

3.1. Poroelastic Materials as non-structural mass

Even though Biot`s theory was established in the middle of the 20th century [10, 11], his findings were not implemented into trim modelling until the 1980s [18, 19, 20]. It was only then, when the application of Biot's theory in vehiccle analysis gained importance with the increasing sophistication of vehicle design.

Despite the difficulty in applying the modelling equations, engineers still desired to approximate the acoustic effects of trims. The earliest approximation was done by adding non-structural mass elements on panels where trims would be installed, which – depending on the model – was sometimes extended with locally increased stiffness and damping values as well. One of the earliest examples of this technique was the work of Priebsch et al. [21]. This study examined noise levels emitted by an inline five-cylinder engine using finite element calculations. Figure 3. shows the engine-crankshaft system's FEM model.
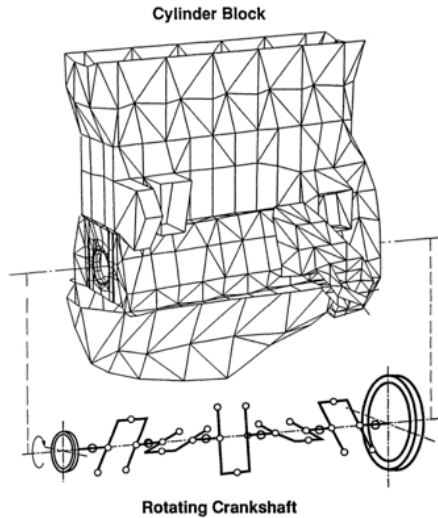
Cylinder Block

Rotating Crankshaft

Figure 3.: finite element model of a 5-cylinder engine and crankshaft [21]

Poroelastic engine trims were modelled as extra mass without influencing the structural properties of the system. As trim elements were not the focus of this study, their effect was not quantified separately, however, the relatively good comparison between simualtion and measurements proved that the non-structural mass idea had merit in this particular application.

While trim elements are used on engines as well, their most prominent acoustic role is in the interior. Various damping mats as well as door cards, instrument panels and the seats themselves are used to attenuate disturbing noise from outside. Therefore, the application of non-structural mass models for interior poroelastic materials was a straightforward choice. An example for such a case is the work done by Sung and colleagues in 1999 [22]. As part of a series of investigations on trimmed bodies, the eigenmodes of a vehicle body were calculated, along with the frequency response. Besides their computational campaign, frequency response functions (FRFs) were also measured, shown on Figure 4. for four different locations.
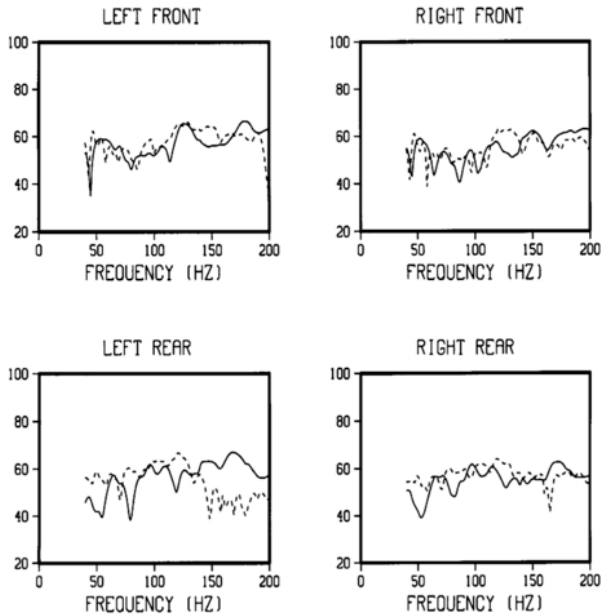
Figure 4.: Comparison of measured (dashed line) and calculated (solid line) SPL [22]

Using 24 reference points over the vehicle body and a single excitation input location, a spatially averaged FRF was compared with the calculated values (Fig. 4). As this was an early attempt at a trimmed body investigation, quite a number of simplifying assumptions were made during the simulation. Trim elements were represented only as non-structural masses, while the doors, hood and trunklid were reduced to point masses and replaced with rigid elements, joined to the bodywork through coupling factors. The relatively small amount of cells (35000 for the body model and 2500 for the acoustic cavity) also reduced accuracy, which manifested itself in the results. Trends were captured correctly, but – especially with increasing frequency – differences between measured and calculated results reached more than 5 dB both in FRF and sound pressure levels inside the cabin.

While this method has a lot of limitations in such a complex case, its quick computation time warrants its use in certain campaigns where short turn-around times are required. Subramanian et al. [23] performed a damping material optimization on a full-size truck cabin. Using a finite element solver, strain energy contours were calculated for treated body panels (Fig. 5). The contours were used to

identify extreme energy points, where treatment was increased. By running this process in a feedback loop, the optimization was completed. Although the accuracy of the results was not perfect, the identified locations and treatment increases were proven useful later in the product development cycle. The overall goal of the optimization was achieved, as the production model received a damping treatment with reduced volume and mass.
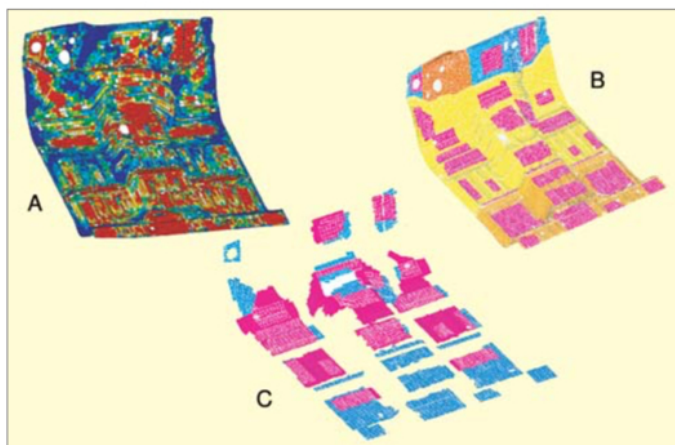
Figure 5.: Composite strain energy contour (A) and optimized damping layer treatment of a vehicle floor panel [23]

Despite being useful in predicting trends, this approximate method has very limited usage. As Nefske [24] also points out, its main advantage is the quick computational time and relatively good correlation with measurements below 50 Hz. Such limited frequency range means that it cannot be reliably used for interior noise assessments.

3.2. Biot-theory in Finite Element Methods

As computational capacities have grown exponentially, the more complex poroelastic formulations started to receive more popularity. One of the earliest to approach the Biot theory in Finite Element Methods was Panneton and Atalla [25]. Their 1995 paper describes a method where the Biot equations are formulated for a finite element solution approach, but simplified by mathematically separating the independent fluid and solid degrees of freedom and approximating the low-frequency material behaviour on the basis of air properties. Despite the mathematical efficiency, the method was only used in the 100-500 Hz region on a geometrically simple model seen on Fig. 6., and no practical application of this exact scheme was

published. Göransson [26] also attempted a simplified FE solution of Biot`s equations by taking advantage of matrix symmetries between porous frame and pore fluids. The fully symmetric formulation, however, still requires five unknowns per node to solve for poroelastic effects, which is why its use is not shown in the paper above 160 Hz.
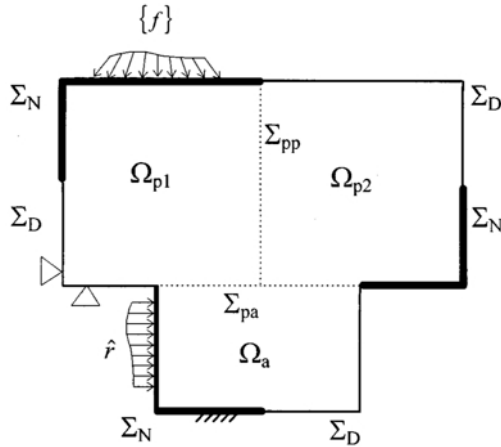

Figure 6.: Geometric setup of the problem tackled by Panneton and Atalla [25]

Deckers et al. [27] provides an excellent summary of the various formulations of the Biot-theory and their numerical applications into a solution scheme. As the goal of this paper was to review practical applications in vehicle industry, the work done by Deckers and colleagues will not be discussed in detail, however it is important as a milestone for summarizing the possible numerical ways to include poroelastic modelling. They also detail various approximation schemes, where either the PEM matrix is assumed to be fully rigid, or an equivalent fluid represents the material. To illustrate the complexity of Biot modelling, Deckers et al. lists seven different formulations that can be used in numerical solvers, with varying numbers of degrees of freedom. Transfer Matrix Method (TMM) is also described as a viable solution for higher frequency problems. Higher frequencies cause problems in FEM simulations due to the small element sizes necessitated by short wavelengths, a problem exacerbated by the presence of porous cavities which further impose wavelength restrictions. TMM alleviates this issue by describing wave propagation through a multi-layered medium. By assuming an infinite number of layers and keeping in mind that only two dilatational and one transversal wave can propagate through a poroelastic medium, the transfer matrix describes the wave field using a limited number of variables. However, the description of the exact coupling system

to the boundaries and originally assuming a plane wave means that TMM`s limitations must be considered.
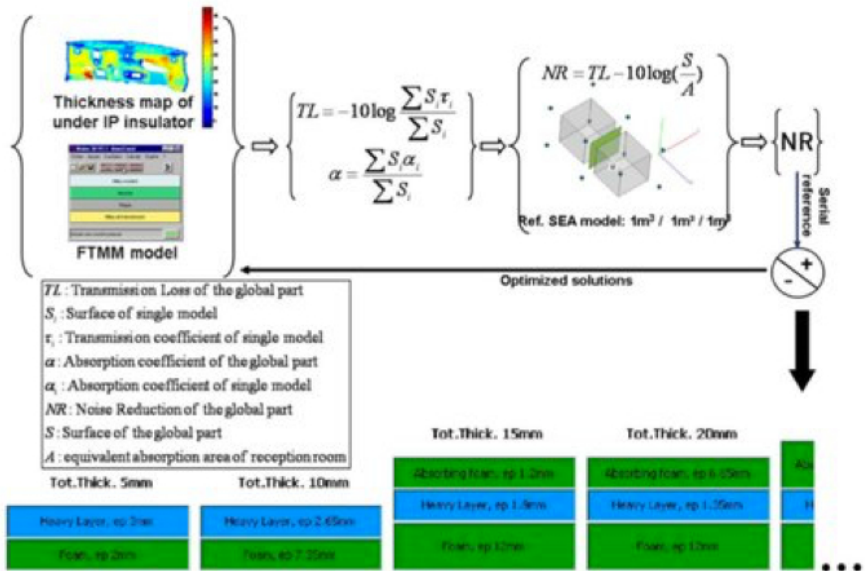
Figure 7.: Optimization loop involving TMM for an instrument panel [28]

Dejaeger et al. [28] used this method in an effective mass optimization study for an instrument panel insulator. Their goal was to retain or improve the acoustic properties of a firewall damping material while reducing its overall weight. Instead of performing detailed analysis of the entire firewall-insulator-instrument panel system in FEM for each iteration with exactly modelled poroelastic effects, the transfer matrix method was used to evaluate multiple concepts in a shorter timeframe, and only the best of those was validated using a complex FE simulation. The optimization loop developed in their paper is shown on Figure 7. Measurements confirmed the validity of the approach, with the optimized insulator providing improved transmission loss as well as lower weight than the baseline configuration. A similar optimization scheme was carried out by Rondeau et al. [29], however on a wider topic breadth: Biot parameter and transmission loss measurements were also carried out on a complex instrument panel model, while the numerical campaign involved FEM, boundary element method and poroelastic modelling as well. Correlation between measurement and simulation was overall good, especially in the above 1000 Hz frequency range, as shown on Fig. 8.

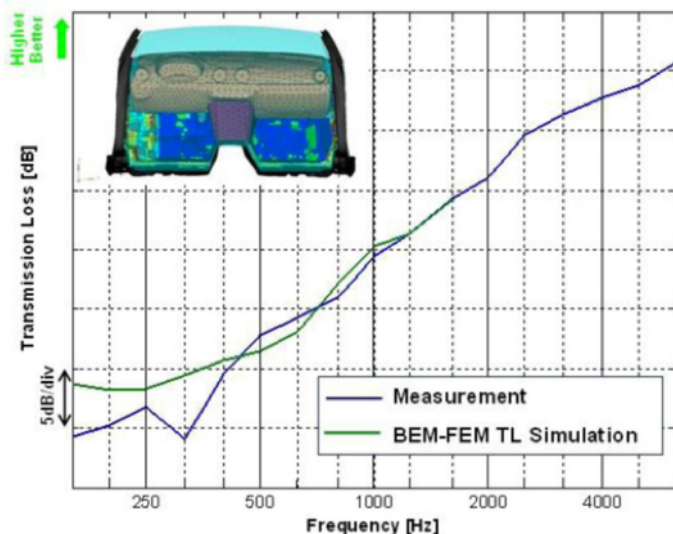*Figure 8.: Transmission loss of instrument panel insulator configuration – measurement and simulation [29]*

While TMM is useful in the component optimization scheme, its limits are reached when dealing with multiple trim elements in a single acoustic system. For a more complex system, Biot equations or a model thereof is needed. In a 2015 publication, Pietrzyk [30] attempted to predict transmitted airborne noise into a vehicle passenger cabin. For the research, a body-in-blue configuration car model was used (no interior trim, doors and enclosures trimmed) with and without porous carpet material. By starting the investigation with a measurement campaign, baseline values were established. Calculations carried out with the porous carpet used the built-in Biot modeler of MSC Actran. Out of the 4 internal microphones, results for the chosen one show questionable accuracy, with differences reaching 10-20 dB in the worst locations. Frequency range was higher here, as expected for airborne noise transmission, however the maximum test frequency was only 400 Hz. Computational results followed measurement curves better in the 0-200 Hz region than above as Fig. 9. shows, although it should be noted that this model needs more refinement to obtain closer results. As mentioned before, the sheer number of material parameters influencing the Biot-model, as well as their frequency dependency can introduce large discrepancies into simulations, and possibly with more correctly set values, this calculation could also arrive at a better conclusion.
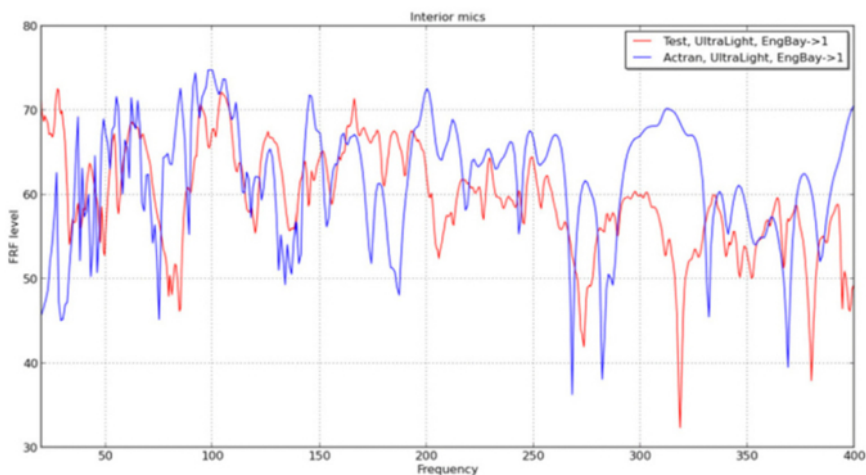
Figure 9.: Resulting FRFs at microphone 1 from measurement (red) and simulation (blue) [30]

   The built-in capabilities of MSC Actran for poroelastic modelling were used by Guellec et al. [31] to perform trim element optimization on a passenger car. As the most recent published work on the FEM-PEM topic, it contains the latest simulation results obtained for a trimmed vehicle setup with floor insulator carpet. Two different calculation methods are presented and compared in their work. One involves MSC NASTRAN for a traditional modal solution, which includes calculation of the reduced impedance matrix in Actran. The other, however, takes place fully in Actran and starts with the computed cavity- and structural modes, with the ability to add frequency dependent damping – either globally, or node by node. As the amount of modes can increase rapidly, only a select number of them are stored for computational efficiency. During the carpet optimization, both solution strategies are used since changing embossments retains the originally calculated impedance matrix, while for changed trim material properties, the NLOPT sequence is used to obtain a new impedance matrix for the original modes. Using the NLOPT model enabled the mass optimization of the trim, and resulted in a 1.7 kg weight gain but 2.5 dB reduced power spectral density level over the whole frequency range up to 250 Hz (Fig. 10.). As future work it is recommended to investigate the high-frequency behavior of the optimized trim and the process itself as well.
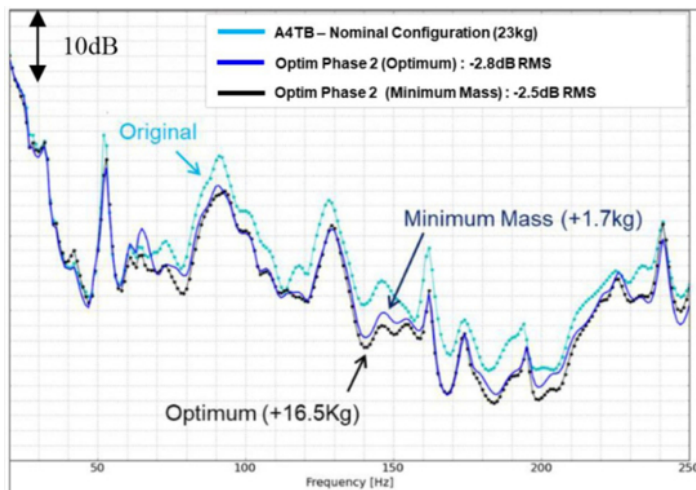
Figure 10.: Trim optimization results showing baseline (light blue), acoustically optimized (dark blue) and minimal mass (black) trim packages [31]

3.3. Hybrid modelling methods

High computational costs arising from the complexity of Biot`s theory have driven engineers to develop alternative methods to account for trim behaviour in acoustic models. Panel acoustic participation is a finite element-based method, as presented by Wang et al. [32]. This method calculates resultant pressures from node vibration, which are summed over each panel to account for their individual pressure contributions. Then, all surrounding panel induced pressures are summed to obtain the resultant pressure for the whole cavity. Thereby the panel participation is defined as the projection of the sound pressure of individual panels in the direction of the overall sound pressure. In their investigation, the panel participation method is used to identify large contributors to interior noise among the panels in contact with the interior cavity on a four seat family car with hammer excitations. Figure 11. shows panel divisions used in the study. Despite good agreement between measurement and simulation, the used frequency range is really narrow (20-50 Hz) and severely limits the applicability of this method.
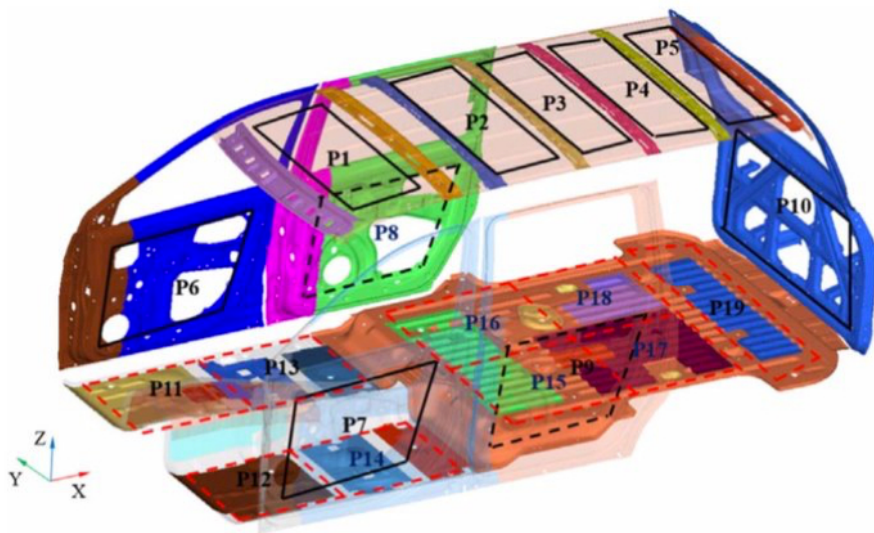
Figure 11.: Panel division in the investigated car for panel acoustic participation method study [32]

Duval and colleagues [33] also worked on an energy based hybrid method to obtain sound pressure levels for a trimmed body. The goal of the study was the implementation of a new sound package for a diesel hatchback car. In order to do so, acoustic power and transfer functions were measured in a fully lined interior with acoustic treatment and used to calculate sound pressure level at the driver`s ear level. The measurements resulted in an acoustic map of the interior, so the optimization could start with the most contributing elements. Figure 12. shows the acoustic power map of the interior panels investigated in the study. Even though the results were quite good, such an optimization relies on measurements on an actual prototype, so it cannot advise designers upstream in the design process.
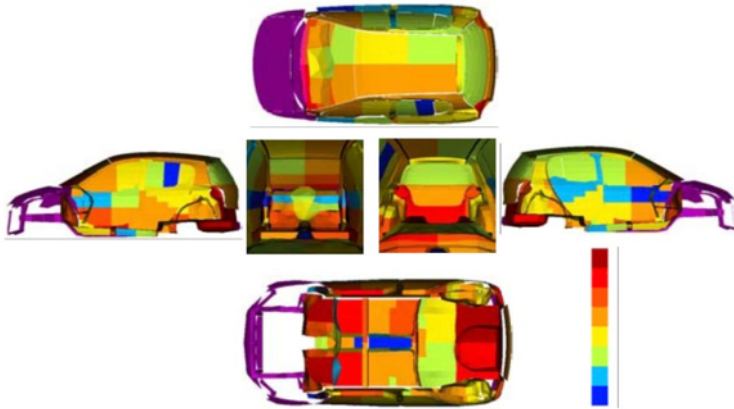
Figure 12.: Acoustic power map of interior trim panels
in a small hatchback car [33]

Not focused on trim elements per se but on an entire design process from high-level targets to execution, Bergen et al. [34] presents a whole development strategy for vehicle manufacturing to deal with the challenge of designing an acoustic sound package. Their recommendation is to use panel participation method (or panel contribution analysis) and transfer path method to establish component goals based on overall design targets, and use more computationally costly procedures like FE models on smaller substructures, so they can be investigated in detail. However, the introduced example is only looking at the finite element results and does not mention the variety of errors that can be introduced into the process at the beginning with the establishment of component goals.

4. Conclusions

An overview of the most relevant literature on Finite Element Method simulations including trim elements made from Poroleastic Materials is given in this paper. Inherent complexities are introduced into an acoustic model once the representation of trim elements is required, since the complex micro-level interaction between fluid and solid phases need to be represented on a macroscopic level. Although Biot`s theory describes this behaviour, it is computationally expensive and introduces an unmanageably large amount of degrees of freedom to handle, especially at higher frequency. Improvements in computing power resulted in the broader application of these methods, and their accuracy is unquestionable below 250 Hz with correct parameters. Despite this, a distinctive lack of higher frequency trim simulations

exists, with no articles citing objectively good correlation between measurement and simulation above the 250-300 Hz region.

Acknowledgements

References

[1] D. Lennström, T. Lindbom, A. Nykänen, Prominence of tones in electric vehicle interior noise. In Internoise 2013 : Noise Control for Quality of Life, 1 (2013) pp. 508–515, Innsbruck: ÖAL Österreichischer Arbeitsring für Lärmbekämpfung.
URL http://urn.kb.se/resolve?urn=urn:nbn:se:ltu:diva-37567

[2] G. Koners, R. Lehmann, Investigation of Tire-Road Noise with Respect to Road Induced Wheel Forces and Radiated Airborne Noise, SAE International Journal of Passenger Cars - Mechanical Systems, 7 (3) (2014) pp. 1194–1197.
doi: 10.4271/2014-01-2075

[3] O. C. Zienkiewicz, R. L. Taylor, The Finite Element Method. Butterworth-Heinemann, Oxford, 2003.

[4] T. J. R. Hughes, The Finite Element Method: Linear Static and Dynamic Finite Element Analysis, Dover Publications, New York, 2007.

[5] S. Marburg, B. Nolte, Computational Acoustics of Noise Propagation in Fluids: Finite and Boundary Element Methods, Springer, New York, 2008.

[6] F. Ihlenburg, Finite Element Analysis of Acoustic Scattering, Springer, New Yoek, 1998.

[7] C. K. Song, J. K. Hwang, J. M. Lee, J. K. Hedrick, Active Vibration Control for Structural–Acoustic Coupling System of a 3-D Vehicle Cabin Model, Journal of Sound and Vibration, 267 (4) (2003) pp. 851–865.
doi: 10.1016/s0022-460x(02)01553-5

[8] S. H. Kim, J. M. Lee, M. H. Shung, Structural-Acoustic Modal Coupling Analysis And Application To Noise Reduction In A Vehicle Passenger Compartment, Journal of Sound and Vibration, 225 (5) (1999) pp. 989–999.
doi:10.1006/jsvi.1999.2217

[9] J.F. Allard, N. Atalla, Propagation of Sound in Porous Media, John Wiley & Sons Ltd, New Jersey, 2009.

[10] M. A. Biot, Theory of Propagation of Elastic Waves in a Fluid-Saturated Porous Solid. I. Low-Frequency Range, The Journal of the Acoustical Society of America, 28 (2) (1956) pp. 168–178. doi: 10.1121/1.1908239

[11] M. A. Biot, Theory of Propagation of Elastic Waves in a Fluid-Saturated Porous Solid. II. Higher Frequency Range, The Journal of the Acoustical Society of America, 28 (2) (1956) pp. 179–191. doi: 10.1121/1.1908241

[12] D. L. Johnson, J. Koplik, R. Dashen, Theory of Dynamic Permeability and Tortuosity in Fluid-Saturated Porous Media, Journal of Fluid Mechanics, 176 (1) (1987) pp. 379-402. doi: 10.1017/s0022112087000727

[13] Y. Champoux, J-F. Allard, Dynamic Tortuosity and Bulk Modulus in Air-Saturated Porous Media, Journal of Applied Physics, 70 (4) (1991) pp. 1975–1979. doi: 10.1063/1.349482

[14] N.-E. Hörlin, N. Nordström, P. Göransson, A 3-D Hierarchical Fe Formulation Of Biots Equations For Elasto-Acoustic Modelling Of Porous Media, Journal of Sound and Vibration, 245 (4) (2001) pp. 633–652. doi: 10.1006/jsvi.2000.3556

[15] S. Rigobert, N. Atalla, F. C. Sgard, Investigation of the Convergence of the Mixed Displacement-Pressure Formulation for Three-Dimensional Poroelastic Materials Using Hierarchical Elements, The Journal of the Acoustical Society of America, 114 (5) (2003) pp. 2607-2617. doi: 10.1121/1.1616579

[16] N. Atalla, M. A. Hamdi, R. Panneton, Enhanced Weak Integral Formulation for the Mixed (u_,p_) Poroelastic Equations, The Journal of the Acoustical Society of America, 109 (6) (2001) pp. 3065–3068. doi: 10.1121/1.1365423

[17] N. Atalla, F. Sgard, C. K. Amedin, On the Modeling of Sound Radiation from Poroelastic Materials, The Journal of the Acoustical Society of America, 120 (4) pp. 1990- 1995. doi: 10.1121/1.2261244

[18] N. Kagami, N. Honda, K. Nishio, Analysis of Booming Noise in Van-Type Vehicle by Component Mode Synthesis Method, SAE International Congress and Exposition, Technical Paper, 1988. doi: 10.4271/880079

[19] M. A. Hamdi, L. Mebarek, A. Omrani, Integration of Acoustic Absorbing Porous Components in Vehicle Environment Using a Novel Finite Element Solver, Journal of the Canadian Acoustical Association, 28 (3) (2000) pp. 24-28.

[20] M. A. Hamdi, L. Mebarek, A. Omrani, N. Atalla, M. Fortez, G. Crignon, S. Lullier, An Efficient Finite Element Formulation for the Analysis of Acoustic and Elastic Waves Propagation in Sound Packages, SAE Transactions, Journal of Passanger Car: Mechanical Systems Journal 110 (6) (2001) pp. 1481–1488. URL: www.jstor.org/stable/44731003

[21] H. H. Priebsch, J. Affenzeller, G. Kuipers, Structure Borne Noise Prediction Techniques, SAE International Congress and Exposition, Technical Paper, 1990. doi: 10.4271/900019

[22] S. H. Sung, D. J. Nefske, H. Le-The, F. Bonarens, Development and Experimental Evaluation of a Vehicle Structural-Acoustic Trimmed-Body Model SAE Noise & Vibration Conference & Exposition, Technical Paper, 1999. doi: 10.4271/1999-01-1798

[23] S. Subramanian, R. Surampudi, K. R. Thomson, S. Vallurupalli, Optimization of Damping Treatment for Structure Borne Noise Reduction, SAE 2003 Noise & Vibration Conference and Exhibition, Technical Paper, 2003. doi:10.4271/2003-01-1592

[24] S. H. Sung, D. J. Nefske, Assessment of a Vehicle Concept Finite-Element Model for Predicting Structural Vibration, SAE 2001 Noise & Vibration Conference & Exposition, Technical Paper, 2001. doi: 10.4271/2001-01-1402

[25] R. Panneton, N. Atalla, An Efficient Finite Element Scheme for Solving the Three-Dimensional Poroelasticity Problem in Acoustics, The Journal of the Acoustical Society of America, 101 (6) (1997) pp. 3287–3298. doi: 10.1121/1.418345

[26] P. Göransson, A 3-D, Symmetric, Finite Element Formulation of the Biot Equations with Application to Acoustic Wave Propagation through an Elastic Porous Medium, International Journal for Numerical Methods in Engineering, 41 (1) (1998) pp. 167–192. doi: 10.1002/(sici)1097-0207(19980115)41:1<167::aid-nme285>3.0.co;2-t

[27] E. Deckers, S. Jonckheere, D. Vandepitte, W. Desmet, Modelling Techniques for Vibro-Acoustic Dynamics of Poroelastic Materials, Archives of Computational Methods in Engineering, 22 (2) (2014) pp. 183–236. doi: 10.1007/s11831-014-9121-0

[28] L. Dejaeger, J.-F. Rondeau, P. Chanudet, B. Auffray, Transmission Loss trim FEM simulation of lightweight automotive dashboard insulators with consideration of the in- strument panel, Acoustics 2012, Nantes, France, 2012. HAL Id: hal-00810732

[29] J. Rondeau, L. Dejaeger, A. Guellec, A. Caillet, L. Bischoff, Cockpit Module Analysis Using Poroelastic Finite Elements, SAE 8th International Styrian Noise, Vibration & Harshness Congress: The European Automotive Noise Conference, Technical Paper, 2014-01-2078, 2014. doi: 10.4271/2014-01-2078

[30] A. Pietrzyk, Prediction of Airborne Sound Transmission into the Passenger Compartment, SAE 2015 Noise and Vibration Conference and Exhibition, Technical Paper 2015-01-2266, 2015. doi: 10.4271/2015-01-2266

[31] A. Guellec, M. Cabrol, J. Jacqmot, B. Van den Nieuwenhof, Optimization of Trim Component and Reduction of the Road Noise Transmission Based on Finite Element Methods, 10th International Styrian Noise, Vibration & Harshness Congress: The European Automotive Noise, Technical Paper 2018-01-1547, 2018. doi: 10.4271/2018-01-1547

[32] Y. Wang, C. Lu, X. Qin, S. Huang, G. Fu, X. Ni, Analysis and Control of Structure-Borne Noise for a Trimmed Body by Using Panel Acoustic Participation Method, Thin-Walled Structures, 119 (2017) pp. 828–838. doi: 10.1016/j.tws.2017.08.001

[33] A. Duval, Vehicle Acoustic Synthesis Method: A Hybrid Approach to Simulate Interior Noise of Fully Trimmed Vehicles, Confort automobile et ferroviaire, Faurecia Vehicle Acoustic Synthesis Method (2004) pp. 1-12.

[34] B. Bergen, N. Schaefer, K. Van de Rostyne, T. Keppens, Vehicle Acoustic Performance Analysis towards Effective Sound Package Design in Mid-Frequency, 10th International Styrian Noise, Vibration & Harshness Congress: The European Automotive Noise, Technical Paper 2018-01-1495, 2018, doi: 10.4271/2018-01-1495

Investigation of Used Engine Oil Lubricating Performance Through Oil Analysis and Friction and Wear Measurements

A. L. Nagy[1], J. Knaup[2], I. Zsoldos[1]

[1]**Széchenyi István University
Egyetem tér 1., 9026, Győr, Hungary
E-mail: nagy.andras1@sze.hu**

[2]**Audi Hungaria Zrt.
Audi Hungária út 1., 9027, Győr, Hungary**

Abstract: Engine oil degradation during long-term engine operation is a well-researched topic, however, the effect of biofuels and synthetic compounds is not fully understood. In order to characterise novel fuel related phenomena in an engine a basis of studies should be established with state-of-the-art engines and conventional fuels and lubricants. This study aims at describing the behaviour of used engine oils throughout their service life based on friction and wear measurements with oil samples from three identical light-duty direct injection supercharged diesel engines. Oil samples were taken from each engine every 50 hours between oil changes to determine physical properties and chemical composition. Friction and wear measurements were conducted on a high-frequency reciprocating rig. The results show strong correlation between oil service life and boron content, as well as acid number and base number. A similar correlation between coefficient of friction with used samples and boron content as well as soot content was observed. A simple model based on a polynomial fitting function was proposed to predict friction and wear from boron content, total acid number and total base number.

Keywords: *engine oil degradation, friction, wear, lubrication*

1.   Introduction

The lubricant in an engine serves multiple purposes, which demands a complex formulation in order to fulfil its function. Aside from friction and wear reduction the oil protects engine parts against corrosion and oxidation, removes third bodies from sliding pairs, transfers heat away from core engine components and helps in achieving appropriate sealing and reducing vibration.

The engine oil composes of a base oil and an additive package [1]. Modern engine oils are mostly polyalphaolefin based, which has inferior properties as a lubricant, hence a selection of additives is needed to achieve the desired function. The most common additives are anti-wear, anti-oxidant, dispersant, detergent, friction modifier, viscosity modifier, extreme pressure agent, anti-foaming agent and emulsifier compounds [2]. A certain property can be achieved through different chemical compounds, but the interaction and compatibility of these compounds with each other must be considered during the formulation of the lubricant.

An engine oil encounters elevated temperatures, high mechanical load, multiple chemically active solids and gases and foreign contaminants during its service life which can contribute to its degradation [3]. Therefore, the lubricant needs to be changed several times during the lifetime of the engine [4]. The main reason of oil degradation is oxidation through the O_2 content of fresh intake air and exhaust gas. The rate of oxidation will increase with rising temperature, which can also lead to the formation of peroxides and free radicals in the engine oil, which in turn can contribute to acid and sludge formation. Oxidation can also lead to an increase in viscosity due to polymerization between the base oil molecules.

State of the art passenger car and commercial vehicle engines implement direct injection fuel systems with high injection pressures and varied injection timing strategies. Injecting fuel directly inside the combustion chamber offers a more precise control over mixture formation and the combustion process which together with charging allows for higher specific power and torque, but also increases the phenomenon of fuel transport through the piston ring package [5], [6], [7]. Fuel and fuel derivatives can contaminate the engine oil and cause further degradation mechanisms. Unburden hydrocarbons can get into the engine oil from the combustion chamber through blow-by gases. Defective injectors, bad fuel spray orientation and

increased gaps between the piston, piston rings and cylinder wall due to wear may cause increased fuel transport into the crankcase. Fuel dilution can cause lubrication issues [8], although in normal operating conditions without any fuel line malfunction the fuel content of the engine oil should stay at a manageable level due to evaporation at higher operating temperatures [9]. However, biofuels can alter these tendencies [10].

The goal of this study is to describe the condition of the engine oil at consequent stages of use and to predict the behaviour of a specific engine oil after a given service life regarding friction and wear through chemical analysis of oil samples from three identical light-duty direct injection supercharged diesel engines.

2. Methodology

Three identical series production turbocharged direct injection diesel engines with a specific power of 60 kW/l were investigated on an engine test bed. Each engine was subjected to a different test cycle with moderate to high loads and engine speeds. The engines were filled with a commercially available SAE 0W-30 grade fully synthetic lubricant with an oil change period of 250 hours. Oil samples were taken every 50 hours for oil condition monitoring purposes and sent to oil analysis. All engines were fuelled with EN 590 compliant regular diesel fuel during the test runs.

The first test cycle (C1) is intended to simulate the conditions of real-life driving and consist of mixed loads and engine speeds. The second test cycle (C2) is designed to stress the exhaust gas recirculation system of the engine and consists of discrete steps with varying engine speeds and throttle positions. The third test cycle was designed to stress the engine to its limits and consist of differing engine speeds with wide-open throttle and half-load conditions.

A total of 43 oil samples were collected and sent to oil analysis in order to characterize the state of used engine oils. Kinematic viscosity at $40\,°C$ and $100\,°C$ were determined according to ASTM D 7279-16 [11]. Acid number and base number were determined through potentiometric titration according to ASTM D 664-11a [12] and ASTM D 2896-15 [13], respectively. Additive content was determined through inductively decoupled plasma atomic emission spectroscopy according to

ASTM D 5185-13e1 [14]. Soot content was determined through infrared spectrometry according to DIN 51452 [15]. Wear metal content was determined through analytical ferrography. Oil samples were homogenised before analysis. A comprehensive list of measured oil properties is given in Table 1.

Table 1. Measured properties of oil samples with their respective units

Property type	Property [unit]		
General	ELh [h]	OAh [h]	OCI [-]
Physical	KV40 [mm^2/s]	KV100 [mm^2/s]	
Chemical	TAN [mgKOH/g]	TBN [mgKOH/g]	
Contaminant	ST [%]	Na [mg/kg]	Si [mg/kg]
Wear metal	Al [mg/kg]	Cr [mg/kg]	Cu [mg/kg]
	Fe [mg/kg]		
Additive	Ca [mg/kg]	Mg [mg/kg]	P [mg/kg]
	Zn [mg/kg]	S [mg/kg]	B [mg/kg]

Selected oil samples were subjected to friction and wear measurements on a high frequency reciprocating rig in order to determine their lubricating performance. Sample selection was based on oil service life, since not all analysed oils were available for friction testing. To have a representation of in-engine oil degradation a complete series of samples were chosen from each test cycle, which corresponds to 1 sample of 50, 100, 150, 200 and 250 hours oil service life from the same oil charge of each engine. A ball-on-disc model system was utilized with a steel sliding pair for the measurements. Each sample was tested under the same circumstances in two consecutive measurements. To minimize measurement error and maximize reproducibility the testing of the aged oil samples was carried out according to the ISO 19291:2016 [16] standard. Mechanical load, stroke, speed, test duration and other boundary conditions of the measurements are given in Table 2.

Ball and disc test specimens are supplied by Optimol Instruments with material properties and dimensions given in Table 3. In addition to the registered coefficient of

Table 2. Parameters of the load set used for friction and wear experiments

Parameter	Value	Parameter	Value
Lubricant volume [ml]	0.3	Run-in Load [N]	50
Stroke length [mm]	1.0	Run-in Time [s]	30
Frequency [Hz]	50	Normal Load [N]	300
Specimen Temperature [°C]	50	Total Test Time [s]	7230

friction (COF) curves the averaged wear scar diameter (AWSD) of each ball specimen was determined through optical microscopy as an average of two perpendicular diameter measurements. Mean COF values were determined as an arithmetic mean of the friction curve after the run-in period.

Table 3. Properties of the ball and disc specimen used for friction and wear experiments

Specimen	Size [mm]	Material	R_a [μm]	HRC [-]
Ball	$\varnothing$10	100Cr6	0.02 $\pm$0.001	61.5 $\pm$1
Disc	$\varnothing$24 x 7.9	100Cr6	0.047 $\pm$0.003	62

A linear correlation analysis according to Pearson was carried out on the data in order to assess the significance of measured oil properties in relation to the condition and lubricating performance of the oil samples. Oil properties listed in Table 1 were correlated to service life (OAh). Subsequently, the properties of the oil samples subjected to friction and wear measurements were correlated to the mean coefficient of friction and the mean averaged wear scar diameter. The calculated correlation coefficients or r-values lie in the range of [-1, 1]. A strong linear relationship is characterized by an r-value close to |1|, whereas an r-value of 0 suggests no linear relationship between the variables. The p-value determines if the r-value is significantly different from 0. A p-value less than or equal to the significance level

signifies that the correlation is different from 0. A level of significance of 0.05 was chosen for the evaluation of the correlation coefficients based on the corresponding *p*-values. Any oil property with a corresponding *p*-value greater than the level of significance was considered as non-determinate for this study.

3. Results

A correlation analysis of measured oil properties of all oil samples in relation to their service life is shown on Figure 1.
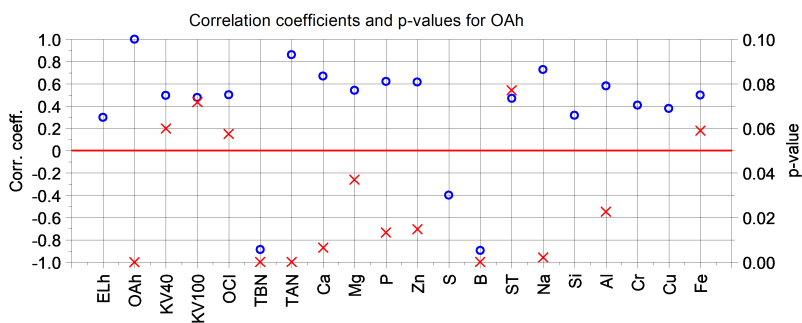
Figure 1. Correlation of measured values to oil service life (OAh); blue circles represent correlation coefficients, red crosses represent p-values, red line represents level of significance (p=0.05)

It suggests that the main indicators of engine oil fitness are TBN, TAN and boron quantity (B) in the oil, signified by low *p*-values and relatively high absolute correlation coefficients (≥ 0.8). A detailed analysis of these values shows a coherent decrease of TBN and boron content as well as a steady increase of TAN with service life of measured samples regardless the test cycle (Fig. 2). In contrast to this behaviour there is noticeable separation in values of the kinematic viscosity of samples from different test cycles. These results are in-line with the expectations, based on the work of other researchers.
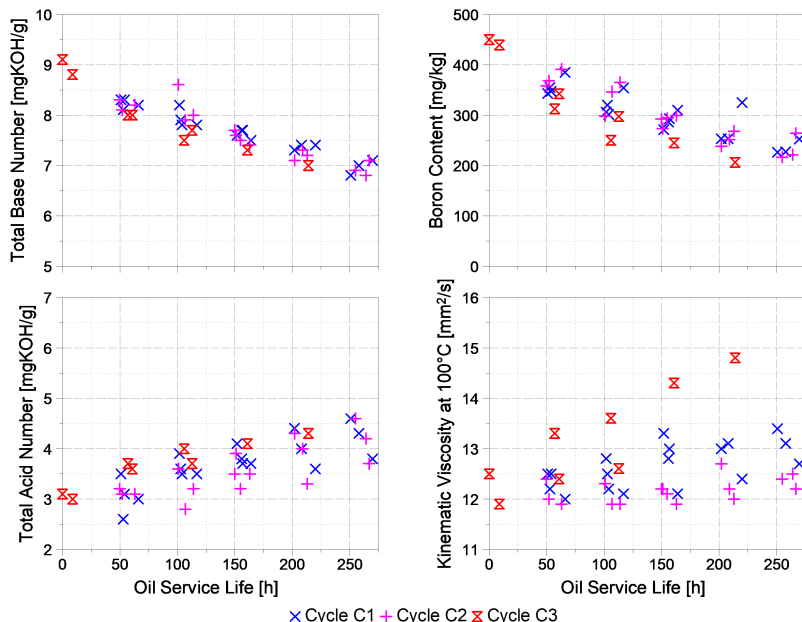
Figure 2. Measured TAN, TBN, boron content and kinematic viscosity at $100\,^{\circ}\text{C}$ *with different oil samples*

A mean value from the coefficient of friction curve as well as the averaged wear scar diameter of each measurement was calculated and correlated to the values from the lubricant analysis. The analysis shows a strong correlation between the boron content, soot content and TBN of the samples to the mean coefficient of friction during friction and wear testing (Fig. 3). As for the amount of wear a similar trend can be observed. Boron content and TBN show a remarkable correlation alongside with TAN. These findings seem to be in accordance with the results of used oil analysis in relation to service life.

To determine the relation between said properties the COF and AWSD values of
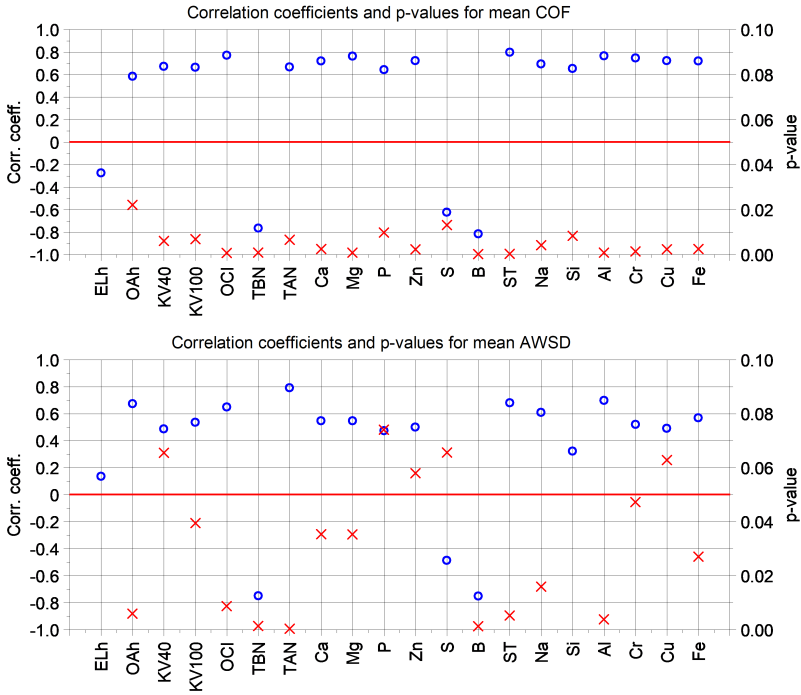
Figure 3. Correlation of measured values to mean COF (upper) and mean AWSD (lower); blue circles represent correlation coefficients, red crosses represent p-values, red line represents level of significance (p=0.05)

individual samples were plotted against boron content, soot content, TAN and TBN respectively (Fig. 4). Apart from COF and soot content, the relation between values appears to be linear. Although it should be noted, that the correlation between the measured coefficient of friction and oil condition is the most apparent on the COF vs. soot content plot.

Based on the presented data, the boron content of the sample together with another
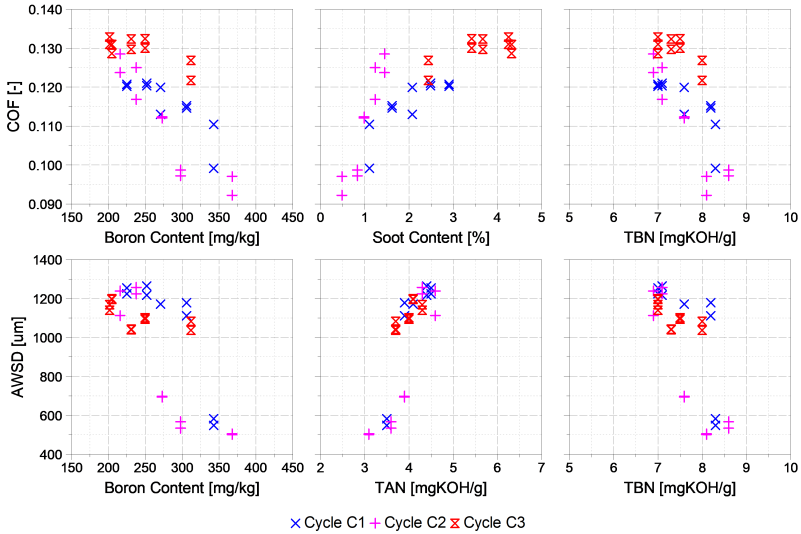
Figure 4. Graphic representation of the relation between used engine oil properties and their performance during friction and wear testing

independent property with significant correlation could be used to describe the fitness of the lubricant in terms of friction reduction and wear protection. A second order polynomial function was found to describe the dependence of COF values from boron and soot content:

$$f(x,y) = p_0 + p_1 \cdot x + p_2 \cdot y + p_3 \cdot x^2 + p_4 \cdot x \cdot y + p_5 \cdot y^2 \qquad (1)$$

where $f(x,y)$ represents the coefficient of friction, x represents boron content and y represents soot content. This with the appropriate coefficients yields an adjusted R-value of 0.9076 and a root-mean-square error (RMSE) of 0.0036. The repeatability of the used friction measurement procedure is 0.012 according to the standard. This means that the proposed function could be successfully used to determine the COF

value from the measured boron and soot content of the sample. In the case of averaged wear scar diameter results the best achievable fit yielded from a similar function, with $f(x,y)$ representing AWSD, x representing TAN and y representing boron content. The best fitting second order polynomial function results in an adjusted R-value of 0.6659 and a RMSE of 157.136 μm, which is far greater than the measurement repeatability of around 70 μm, however lies below the border of reproducibility of around 230 μm.
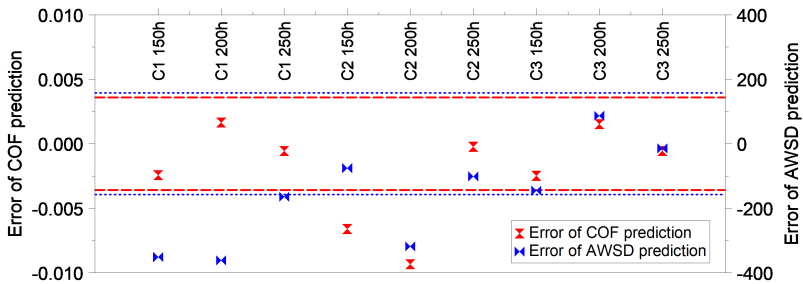
Figure 5. Absolute error of prediction for COF and AWSD with validation dataset; dashed lines represent ± RMSE of the COF prediction model while dotted line represent the same for the AWSD prediction model

A validation dataset consisting of boron, soot and TAN values as well as measured values of COF and AWSD of selected samples was utilized in order to evaluate the fitness of the polynomial models. One samples from each test cycle (C1, C2 and C3) at 150, 200 and 250 hours service life was included in the validation dataset. The absolute difference between predicted and measured COF and AWSD values at the validation data points are depicted on Fig. 5. In the case of the COF model for 7 out of 9 predictions the error is lower than the RMSE of the fit, which can be considered a good accuracy. The AWSD model shows a worse accuracy with only 5 predictions out of 9 with an error lying under the RMSE of the fit.

Due to confidentiality the author will not disclose the coefficients of the polynomial functions.

4.   Discussion

The presented results presume a significant correlation between the TAN, TBN and boron content of a used engine oil and its service life. The acid number is used to measure the concentration of acidic species present in the engine oil. Lean oil has an initial acidity which will increase during service due to acid formation as a result of oxidation and the presence of acidic compounds formed during combustion. The base number measures the alkaline reserve of the lubricant which serves as a neutralizing agent to hinder the effect of weak acids. Therefore the initial base number of a lean oil will decrease during the service life [17]. Boron esters are used in modern formulations as an antioxidant additive or as replacement to ZDDP. Boron can also be used as a solid lubricant nano-additive to successfully reduce friction and wear in a sliding pair as discussed in [18], [19], [20] and [21]. In both cases the initial boron content of the lubricant will decrease with time as experienced. This phenomenon takes place due to degrading chemical reactions and boundary layer formation, which reduce the amount of boron additives in the oil. Hence, the presented results are in accordance with the scientific literature.

The conducted correlation analysis assumed a linear correlation between the investigated properties and service life, as well as coefficient of friction and averaged wear scar diameter. This assumption disregards the possibility of non-linear correlation, which can explain why only a weak fit was achievable with the wear scar diameter. Taking only linear correlations into account was a decision in favour of simplicity, as non-linear behaviour would demand finer sampling of the used oils which was not in the scope of this study. Further experimentation should be considered regarding the dependence of oil properties from the test cycle. Treating this factor as an inherent property of the dataset can introduce an error in the model. A detailed study with real-life driving conditions conducted on a diverse vehicle fleet would be necessary to address this flaw.

It should also be noted that the models presented in this study are only applicable in the case of boron containing engine lubricants, and should not be applied without further consideration to arbitrary engine oils or other lubricants.

5.   Conclusion

In order to describe the friction and wear behaviour of used engine oils a series of measurements was conducted on a high frequency reciprocating rig with oil samples from three identical light-duty series production diesel engines. Each engine was subjected to a different test cycle aiming at simulating different use cases. Oil samples were taken every 50 hours between oil changes and analysed in a laboratory. The results of oil analysis and friction and wear testing showed that a strong correlation exists between oil service life and TAN, TBN and boron content of the sample. These findings are in accordance with the expectations, based on the work of other authors. This correlation was found to be present in connection with the coefficient of friction and average wear scar diameter values as well, although with somewhat lower significance. Based on these findings a simple polynomial fitting model was proposed to predict the COF and AWSD values of a given oil sample without conducting the friction and wear experiments. It should be noted that only linear correlation between oil properties and measured COF and AWSD values was considered, disregarding the possibility of non-linearity between the investigated values. Since boron is not present in the base oil, the presented model approach is only applicable to engine oils containing boron additives.

Acknowledgement

References

[1] M. Torbacke, A. Kassman Rudolphi, E. Kassfeldt, Lubricants: Introduction to Properties and Performance, 1st Edition, Wiley, Chichester, 2014.

[2] L. R. Rudnick, Lubricant Additives Chemistry and Application, 2nd Edition, CRC Press Inc, Boca Raton, FL, USA, 2009.

[3] A. Toms, L. Toms, Oil analysis and condition monitoring, in: R. M. Mortier, M. F. Fox, S. Orszulik (Eds.), Chemistry and Technology of Lubricants, 3rd Edition, Springer Netherlands, Dordrecht, 2010, pp. 459–495.

[4] P. Lacey, S. Gunsel, M. Ferner, M. Pozebanchuk, A. Alim, Effect of oil drain interval on crankcase lubricant quality, SAE Technical Papers `doi:10.4271/ 2003-01-1957`.

[5] T. Sagawa, H. Fujimoto, K. Nakamura, Study of fuel dilution in direct-injection and multipoint injection gasoline engines, in: SAE Technical Paper, SAE International, 2002, pp. 1107–1116. `doi:10.4271/2002-01-1647`.

[6] T. Hu, H. Teng, X. Luo, X. Chen, Impact of Fuel Injection on Dilution of Engine Crankcase Oil for Turbocharged Gasoline Direct-Injection Engines, SAE Int. J. Engines 8 (2015) pp. 1107–1116. `doi:10.4271/2015-01-0967`.

[7] P. J. Shayler, L. D. Winborn, A. Scarisbrick, Fuel transport to the crankcase, oil dilution and hc return with breather flow during the cold operation of a si engine, in: SAE Technical Paper, SAE International, 2000, pp. 1107–1116. `doi:10.4271/2000-01-1235`.

[8] S. Watson, V. Wong, The effects of fuel dilution with biodiesel and low sulfur diesel on lubricant acidity, oxidation and corrosion: A bench scale study with cj-4 and ci-4+ lubricants, in: STLE/ASME 2008 International Joint Tribology Conference, ASME, Miami, 2008, pp. 233–235. `doi:10.1115/ IJTC2008-71221`.

[9] M. Hakeem, J. Anderson, G. Surnilla, S. S. Yamada, Characterization and speciation of fuel oil dilution in gasoline direct injection (di) engines, in: ASME 2015 Internal Combustion Engine Division Fall Technical Conference, ASME, Houston, Texas, USA, 2015. `doi:10.1115/ICEF2015-1072`.

[10] X. He, A. Williams, E. Christensen, J. Burton, R. McCormick, Biodiesel impact on engine lubricant dilution during active regeneration of aftertreatment systems, SAE Int. J. Fuels Lubr. 4 (2011) pp. 158–178. `doi:10.4271/ 2011-01-2396`.

[11] ASTM D7279-16, Standard Test Method for Kinematic Viscosity of Transparent and Opaque Liquids by Automated Houillon Viscometer, Standard, ASTM International, West Conshohocken, PA, USA (2016). `doi:10.1520/D7279-16`.

[12] ASTM D664-11a, Standard Test Method for Acid Number of Petroleum Products by Potentiometric Titration, Standard, ASTM International, West Conshohocken, PA, USA (2011). `doi:10.1520/D0664-11A`.

[13] ASTM D2896-15, Standard Test Method for Base Number of Petroleum Products by Potentiometric Perchloric Acid Titration, Standard, ASTM International, West Conshohocken, PA, USA (2015). `doi:10.1520/D2896-15`.

[14] ASTM D5185-13e1, Standard Test Method for Multielement Determination of Used and Unused Lubricating Oils and Base Oils by Inductively Coupled Plasma Atomic Emission Spectrometry, Standard, ASTM International, West Conshohocken, PA, USA (2013). `doi:10.1520/D5185-13E01`.

[15] DIN 51452, Testing of lubricants; determination of the soot content in used Diesel engine oils; infrared spectrometry, Standard, Deutsches Institut für Normung e. V., Berlin, Germany (1994).

[16] ISO 19291:2016, Lubricants – Determination of tribological quantities for oils and greases – Tribological test in the translatory oscillation apparatus, Standard, International Organization for Standardization, Geneva, Switzerland (2016).

[17] D. J. Smolenski, S. E. Schwartz, Automotive engine-oil condition monitoring, in: E. R. Booser (Ed.), CRC Handbook of Lubrication and Tribology Volume III Monitoring, Materials, Synthetic Lubricants, and Applications, CRC Press, Inc, New York, 1994, pp. 17–32.

[18] H. Baş, Y. E. Karabacak, Investigation of the effects of boron additives on the performance of engine oil, Tribology Transactions 57 (4) (2014) pp. 740–748. `doi:10.1080/10402004.2014.909549`.

[19] J. Sahu, K. Panda, B. Gupta, N. Kumar, P. Manojkumar, M. Kamruddin, Enhanced tribo-chemical properties of oxygen functionalized mechanically exfoliated hexagonal boron nitride nanolubricant additives, Materials Chemistry and

Physics 207 (2018) pp. 412–422. `doi:10.1016/j.matchemphys.2017.12.050`.

[20] Q. Wan, Y. Jin, P. Sun, Y. Ding, Tribological behaviour of a lubricant oil containing boron nitride nanoparticles, Procedia Engineering 102 (2015) pp. 1038 – 1045. `doi:10.1016/j.proeng.2015.01.226`.

[21] L. Wang, H. Wu, D. Zhang, G. Dong, X. Xu, Y. Xie, Synthesis of a novel borate ester containing a phenylboronic group and its tribological properties as an additive in pao 6 base oil, Tribology International 121 (2018) pp. 21–19. `doi:10.1016/j.triboint.2018.01.033`.

Challenges of Digital Twin System

C. Monsone[1], J. Jósvai[2]

[1]Széchenyi István University, Doctoral School of Multidisciplinary Engineering Sciences
Egyetem tér 1, 9026, Győr, Hungary
E-mail: monsone.cristina@sze.hu

[2]Széchenyi István University, Department of Vehicle Manufacturing
Egyetem tér 1, 9026, Győr, Hungary
E-mail: josvai@ga.sze.hu

Abstract: Today's manufacturing and assembly systems have to be flexible to adapt quickly to an increasing number and variety of products. The Industry 4.0 conceptualization has several potentials, i.e. flexibility in business and manufacturing processes, where the intelligent and interconnected systems, in particular the Cyber-Physical Production System (CPPS), play a vital role in the whole lifecycle of eco-designed products. In particular, the CPPS represents a suitable way for manufacturers that want to involve their customers, delivering instructions to machines about their specific orders and follow its progress along the production line, in an inversion of normal manufacturing. The development of Info Communication Technologies (ICT) and Manufacturing Science and Technology (MST) enables the innovation of Cyber-Physical Production Systems. However, there are still important challenges that need to be addressed in particular at technological and data analysis level with the implementation of Deep Learning analysis.

Keywords: *Digital Twin, CPPS, Data, AI, Industry 4.0, IoT, Cloud*

1. Introduction

Industry is one of the pillars of the European economy : the manufacturing sector in the European Union accounts for 2 million enterprises, 33 million jobs and 60% of productivity growth (Eurostat,2018). We stand on the brink of a new industrial revolution, driven by new-generation information technologies such as the Internet of Things (IoT), cloud computing, big data and data analytics, robotics.

They open new horizons for industry to become more efficient, to improve processes and to develop innovative products and services. Recent studies estimate that digitalisation of products and services can add more than EUR 110 billion of annual revenue to the European economy in the next five years. In particular, with the growing deployments of IoT systems, the importance of the concept of a digital avatar - Digital Twin - of a physical thing has gathered significant interest in the recent years. These digital proxies are expected to be built from the domain knowledge of subject matter experts as well as the real time data collected from the devices [1].

The concept of Industry 4.0, or the Fourth Industrial Revolution, has the potential for radically increased system re-configurability and flexibility. At its core, the notion of Cyber-Physical Production System, as the new generation of embedded systems with advanced artificial intelligence and improved communication capabilities, is seen as the key enabling concept that will render production activities more sustainable. This is due to the modular and self-contained nature of cyber-physically formulated equipment and systems that, instead of relying in statically defined and bespoke inter-connections, operate in a more open way by considering dynamically establishing and on-demand interactions between the system components [2] .

The intelligence and adaptiveness attributed to this new class of embedded systems therefore not restricted to the computational capabilities of local controllers/devices and can, as well, harness computationally rich cloud environments. The pursue of new industrial automation concepts and solutions, despite being recently fuelled by the latter initiatives, and related developments, is also backed up by more than 20 year of multidisciplinary research. In particular, digitalisation is related to the Internet of Things (IoT) concept and the convergent development of many other technologies discussed in the Fourth Industrial Revolution (Industry 4.0). As a founding concept, IoT sees all the devices, with embedded sensors, electronics and capabilities to connect to others, as "things". Such things allow to collect and exchange data through internet and, in general, through networks of devices, named as smart objects [3] .

Big Data analytics, that access the data and promise to provide fast decision-making with the use of smart analytics tools, complement the IoT with further features useful for decision-making support. In such a technology landscape, an important concept is often remarked: the Digital Twin (DT), meant as a system's digital counterpart along its lifecycle. The DT can be considered as a virtual entity, relying on the sensed and transmitted data of the IoT infrastructure as well as on the capability to elaborate data by means of Big Data technologies, with the purpose to allow optimizations and decision-making. In this scope, the DT is often overlapped with advanced simulation. Overall, the DT, as a virtual entity, can regard everything of the physical world, thus physical asset can also be directly taken as a target scope of DT modeling (Fig.1)[4].
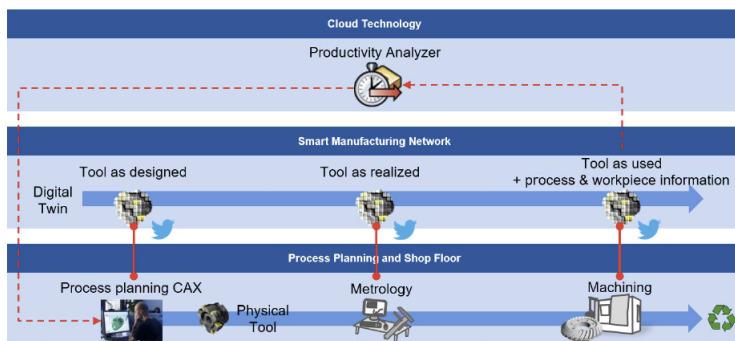
Figure 1. Demonstrator: Digital twin in a production line[5].

2. State of the Art

The CPPS conceptualization dramatically reduces the integration effort by virtually eliminating the need, time, and cost for re-programming. The intelligence and adaptiveness attributed to this new class of embedded systems therefore not restricted to the computational capabilities of local controllers/devices and can, as well, harness computationally rich cloud environments, in a multidisciplinary research domain. These eventually led to several innovative production paradigms and technical contributions namely, i.e. Holonic Manufacturing Systems (HMS) powered by Multiagent

Systems (MAS) and other Artificial Intelligence (AI) techniques. The marriage of digital and physical technologies would affect how customers, consumers, employees, and other parts of the business landscape expect to experience and interact with an organization [4].

Digital twin (DT) is one of the most promising enabling technologies for realizing smart manufacturing and Industry 4.0. DTs are characterized by the seamless integration between the cyber and physical spaces. The importance of DTs is increasingly recognized by both academia and industry. It has been almost 15 years since the concept of the DT was initially proposed. To date, many DT applications have been successfully implemented in different industries, including product design, production, prognostics and health management, and some other fields [5].

Today's manufacturing and assembly systems have to be flexible to adapt quickly to an increasing number and variety of products, and changing market volumes. To manage these dynamics, several production concepts (e.g., flexible, reconfigurable, changeable or autonomous manufacturing and assembly systems) were proposed and partly realized in the past years. In particular, intelligent and interconnected systems play a vital role in the whole lifecycle of eco-designed products and especially for manufacturers that want to involve their customers, delivering instructions to machines about their specific orders and follow its progress along the production line, in an inversion of normal manufacturing [6] .

Based on the collaborative technologies and services mentioned above, the shared workspace between humans and robots can be considered an advanced cyber-physical system, as previous mentioned, the DT. It'is supported by the dynamic control algorithms and online monitoring devices and it's core element is the data acquisition and data evaluation [7].

3.   R&D Challenges

The concept of Industry 4.0, or the Fourth Industrial Revolution, has the potential for radically increased system reconfigurability and flexibility and it's aimed at boosting Europe's economy by delivering sustainable economic and social benefits from a digital single market [1].

This is due to the modular and self-contained nature of CPPS formulated equipment and systems that, instead of relying in statically defined and bespoke interconnections,

operate in a more open way by considering dynamically establishing and on demand interactions between the system components. It is important to notice that the CPPS conceptualization requires a knowledge and data intensive environment as most CPPS components will be collectors and processors.

A Digital Twin can have intelligence. For example, an intelligent product can retrieve information about itself and is capable of participating or making decisions about its own future [8].

Summarizing, several characteristics for an intelligent product are: (a) Requires a global unique identification; (b) Is capable of communicating with its environment; (c) Can retrieve and store data about itself; and (d) Is capable of participating in or making decisions relevant to its own destiny [9]. It is not necessary to have all these characteristics for a Digital Twin, since all these are related to intelligent product. However, some of these characteristics are relevant for the management of the Digital Twin. In particular through CPPS, the development of new business models, new services are expected which may change many aspects of our life. The potential application fields are almost endless: air- and ground-traffic; discrete and continuous production systems; logistics; medical science, energy production, infrastructure surrounding us, entertainment, and we could keep on enumerating[6].

In the coming space only some of the R&D challenges are outlined from the much bigger set of research fields which are related to CPPS. Especially when adopted in manufacturing, the DT has taken a new objective: to simulate the complex behaviour of production systems, also including external factors, as human presence and technical constraints [10]. In particular:

- Data evaluation and acquisition [7].

- Context-adaptive and (at least partially) autonomous systems. Methods for comprehensive, continuous context awareness, for recognition, analysis and interpretation of plans and intentions of objects, systems and participating users, for model creation for application field and domain and for self-awareness in terms of knowledge about own situation, status and options for action are to be developed [6] .

- Cooperative production systems. New theoretical results are to be achieved

and the development of efficient algorithms for consensus seeking, cooperative learning and distributed detection is required[6].

- Improved maintenance decision making (damage / cracks prediction; material geometric / plastic deformation, and reliability modelling of physical systems) [11].

- Checking the feasibility and optimizing the control software of the system [12].

- Simulating the orchestration of IoT devices [13] .

- Human-machine (including human-robot) symbiosis. The development of a geometric data framework to fusion assembly features and sensor measurements and fast search algorithms to adapt and compensate dynamic changes in the real environment is required [6] .

- Statistically-based decision making and optimization, such as optimizing the system's behaviour / performances, by simulating it during the design phase or during other lifecycle phases, knowing its past and present states [14][15].

3.1. Cyber Physical Production System

The concept of a cyber-physical production system (CPPS) is a manufacturing-centered version of a CPS. The CPS includes embedded systems , internet services, management processes. The CPPS fuses computer science (CS), ICT, and manufacturing-science technology. Based on the collaborative technologies and services mentioned above, the shared workspace between humans and robots can be considered an advanced cyber-physical system, which is supported by the dynamic control algorithms and online monitoring devices. In particular, the CPPS will enable and support the communication between humans, machines and products alike (Fig. 2).

The elements of a CPPS are able to acquisition and process data, and can selfcontrol
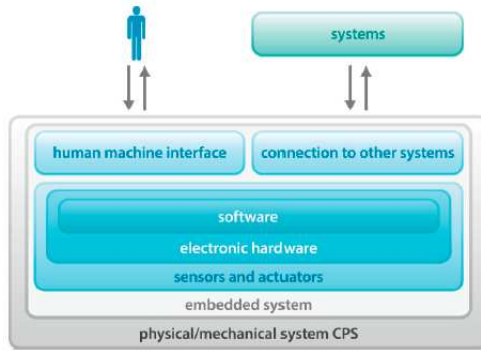
Figure 2. Interaction between Humans and machine in CPS.[6]

certain tasks and interact with humans via interfaces. CPPS partly break with the traditional automation pyramid (left side of Fig. 3).
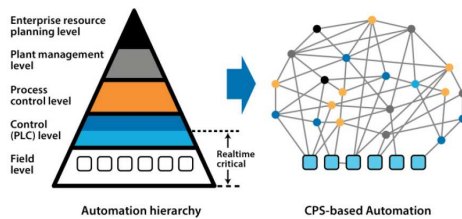
Figure 3. Decomposition of automated hyerarchy with distributed services.[6]

The typical control and field levels still exist which includes common PLCs close to the technical processes to be able to provide the highest performance for critical control loops, while in the other, higher levels of the hierarchy a more decentralized way of functioning is characteristic in CPPS[6].
Currently, the CPPS concept is still under development. In the area of asset management, CPPS has the potential to provide self-awareness and self-maintenance

capabilities. The implementation of predictive analytics as part of the CPPS framework enables the assets to continuously track their own performance and health status and predict potential failures. By implementing this predictive analytics along with a decision support system, proper services could be requested and actions taken to maximize the uptime, productivity and efficiency of the industrial systems. CPPS, as the central hub for data management in fleet level, plays a critical role in achieving the above-mentioned goals[16].

3.2. Digital Twin

Thanks to the CPPS and AI platform, a radically increased system where the re- configurability and flexibility allows a predictive planning and control in order to prevent and solve the potential failure in a production or in a physical system . Indeed , the technological basis of Industry 4.0 roots back in the Internet of Things (IoT),which proposed to embed electronics, software, sensors, and network connectivity into devices (i.e. ”things”), in order to allow the collection and exchange of data through the internet[16] [17].

As such, IoT can be exploited at industrial level: devices can be sensed and controlled remotely across network infrastructures, allowing a more direct integration between the physical world and virtual systems, and resulting in higher efficiency, accuracy and economic benefits. Although it is a recent trend, Industry 4.0 has been widely discussed and its key technologies have been identified among which Cyber-Physical Production Systems (CPPS) have been proposed as smart embedded and networked systems within production systems[18] .

They operate at virtual and physical levels interacting with and controlling physical devices, sensing and acting on the real world [19]. According to scientific literature, in order to fully exploit the potentials of CPPS and IoT, proper data models should be employed, such as ontologies which are explicit, semantic and formal conceptualizations of concepts in a domain [20][21][22].

They are the core semantic technology providing intelligence embedded in the smart CPPS and could help the integration and sharing of big amounts of sensed data [23] [24]. Through the use of Big Data analytics, it is possible to access sensed data, through smart analytics tools, for a rapid decision making and improved productivity[25]. The Digital Twin (DT) is meant as the virtual and computerized counterpart of a physical system that can be used to simulate it for various purposes, exploiting a

real-time synchronization of the sensed data coming from the field; such a synchronization is possible thanks to the enabling technologies of Industry 4.0 and, as such, the DT is deeply linked with it [26].

The DT was first born in the aerospace field - the first definition of the DT was forged by the NASA as "an integrated multi-physics, multi-scale, probabilistic simulation of a vehicle or system that uses the best available physical models, sensor updates, fleet history, etc., to mirror the life of its flying twin. It is ultra-realistic and may consider one or more important and interdependent vehicle systems": this definition first appeared in the draft and after in the final release of the NASA " Modeling, Simulation, Information Technology Processing Roadmap" in 2010 and only recently has been adopted also in manufacturing contexts: such a term is used in industrial environments and in governmental research initiatives. However, scientific literature that describes the contextualisation of the concept in the manufacturing domain is still at its infancy [27].

Digital twins are becoming a business imperative, covering the entire lifecycle of an asset or process and forming the foundation for connected products and services and allows analysis of data and monitoring of systems to head off problems before they even occur, prevent downtime, developing, in a cloud-based system, new opportunities and even plan for the future by using simulations, thinking of a digital twin as a bridge between the physical and digital world[28].

However, Industry 4.0 is a multi-faceted problem, and it is unlikely that all aspects of it will be applicable to all businesses. Whilst the area of Intelligent Manufacturing is itself a multifaceted problem, the recurring element that underpins much of this revolution is the collection, utilization and understanding of data, or the study of 'Informatics'; almost all of the areas linked with the intelligent manufacturing research area rely on the capture and analysis of data in some way.

To this end the use of advanced data analytics and machine learning is a key technology to develop to further these other technologies; and the next step in this chain lies in utilizing the vast reserves of data through data mining and knowledge discovery, to better understand these manufacturing processes[28][29].

4.   Methodologies

Cyber Physical Production Systems (CPPS) have been proposed as a key concept of Industry 4.0 architectures. A CPPS can be described as a set of physical devices, objects and equipments that interact with a virtual cyberspace through a communication network. Each physical device will have its cyber part as a digital representation of the real device, culminating in the "Digital Twin". So, the Digital Twin can monitor and control the physical entity, while the physical entity can send data to update its virtual model [28] [30].

4.1.   Data acquisition

The Digital Twin model can be composed by different kind of models and data, but for its the realization the following two main systems are introduced for data acquisition: sensor based tracking and machine vision. In particular, the new advanced methodologies considers AutomationML and Deep Convolutional Neural Network (DCNN)[27] [28] [30].

- AutomationML
  The AutomationML is considered one of the best solution for the DT because it stores engineering information following the object-oriented paradigm and allows the modelling of physical and logical plant components as data objects en-capsulating different aspects . An object may consist of other sub-objects, and may itself be a part of a larger composition or aggregation [19]. The AutomationML defines Computer Aided Engineering Exchange (CAEX) as a meta model for the storage and exchange of engineering models. The topics below, summarizes its parts and the way it is used to create models [28].
  - Creates a hierarchy of components, called Instance- Hierarchy (IH), from the top-level down to single components (InternalElements, IEs) with interfaces (External Interfaces, EIs) and relations (Internal Links, ILs),
  - Reusable System Unit Classes (SUCs) defining component types.
  - Reusable Interface Classes (ICs) for specifying connection points of RCs (Role Classes), SUCs and the interface type of EIs,

    – Attributes for describing characteristics of each previously introduced modeling element. By definition, CAEX supports object-oriented modeling for all of these aspects. External Interfaces describing System Unit Classes instances are connected by Internal Links via External Interfaces, which in turn are instances of Interface Classes [29].

Another way is represented by the utilisation of a Deep Learning techniques, in particular Deep Convolutional Neural Network (DCNN), for the data aquisition , especially where also the aspect of the product is a crucial element in the production line.

- Deep Convolutional Neural Network (DCNN)

    In the field of the Deep Learning (DL) the pre-trained Deep Convolutional Neural Network (DCNN) model with transfer learning have shown to be highly effective in processing visual data, such as images and videos. DCNNs take raw input data at the lowest level and transforms them by processing them through a sequence of basic computational units to obtain representations that have intrinsic values for classification in the higher layers [30].

The use of models allows that a user, without knowledge about programming, to model a Digital Twin of the equipment that he operates and create models to exchange data between systems.

5.   Conclusion

The marriage of digital and physical technologies would affect how customers, consumers, employees, and other parts of the business landscape expect to experience and interact with an organization. While the technologies associated with Industry 4.0 - from robotics to the Internet- of-Things, and from big data analytics to artificial intelligence - are transforming business processes, an often-overlooked challenge is managing the inevitable shift in workplace dynamics, which is crucial to supporting

the successful integration of Industry 4.0 technologies. As presented in this paper, we have demonstrated that the : one of the key requirements is realizing a real-world production environment that comprises the characteristics of a cyber- physical production system in relation to the data availability and data analysis through AI techniques . Thanks to the Digital Twin, the aim is to allow production models to be implemented using captured near-real time data to improve the production monitoring and to be designed to include the possibility to flexibly configure all of the control-relevant methods and parameters in the production environment. Within this context, it was shown that in terms of attaining production objectives and increasing an enterprise's competitiveness, there is generally tremendous potential both in compiling, supplying and analyzing operational data. As reported in the previuos paragraph, the CPPS and AI platform - through Digital Twin - represents a radically increased system where the re-configurability and flexibility allows a predicitive planning and control in order to prevent and solve the potential failure in a production or in a physical system. In particular, it emerged that the relevance of Digital Twin (DT) for manufacturing industry lies in their definition as virtual counterparts of physical devices. These are digital representations based on semantic data models that allow running simulations in different disciplines, that support not only a prognostic assessment at design stage (static perspective), but also a continuous update of the virtual representation of the object by a real time synchronization with sensed data. This allows the representation to reflect the current status of the system and to perform real-time optimizations, decision making and predictive maintenance according to the sensed conditions.

References

[1] Digitisation Research and Innovation - Transforming European industry and services, August 2017.
`https://publications.europa.eu/en/publication-detail/`
`-/publication/662617ce-d4b9-11e7-a5b9-01aa75ed71a1/`
`language-en`

[2] K. Ashton, That 'internet of things' thing, RFID journal, 22 (7) (2009) pp. 97-114.

[3] L. Atzori, A. Iera, G. Morabito, The internet of things: A survey, Computer networks, 54 (15) (2010) pp. 2787-2805.

`doi:10.1016/j.comnet.2010.05.010`

[4] F. Tao, H. Zhang, A. Liu, A. Y. Nee, Digital twin in industry: state-of-the-art, IEEE Transactions on Industrial Informatics, 15 (4) (2018) pp. 2405-2415.
`doi:10.1109/TII.2018.2873186`

[5] D. Botkina, M. Hedlind, B. Olsson, J. Henser, T. Lundholm, Digital twin of a cutting tool, Procedia CIRP, 72 (2018) pp. 215-218.
`doi:10.1016/j.procir.2018.03.178`

[6] L. Monostori, Cyber-physical production systems: Roots, expectations and RD challenges, Procedia Cirp, 17 (2014) pp. 9-13.
`doi:10.1016/j.procir.2014.03.115`

[7] T. H. J. Uhlemann, C. Lehmann, R. Steinhilper, The digital twin: Realizing the cyber-physical production system for industry 4.0, Procedia Cirp, 61 (2017) pp. 335-340.
`doi:10.1016/j.procir.2016.11.152`

[8] B. Dworschak, H. Zaiser, Competences for cyber-physical systems in manufacturing–first findings and scenarios, Procedia CIRP, 25 (2014) pp. 345-350.
`doi:10.1016/j.procir.2014.10.048`

[9] K. Hribernik T. Wuest, K. D. Thoben, Towards Product Avatars Representing Middle-of-Life Information for Improving Design, Development and Manufacturing Processes, in: G. L. Kovács, D. Kochan (eds) Digital Product and Process Development Systems. NEW PROLAMAT 2013. IFIP Advances in Information and Communication Technology, vol 411. Springer, Berlin, Heidelberg, 2013, pp. 85-96.
`doi:10.1007/978-3-642-41329-2_10`

[10] R. Rosen, G. Von Wichert, G. Lo, K. D. Bettenhausen, About the importance of autonomy and digital twins for the future of manufacturing, IFAC-PapersOnLine, 48 (3) (2015) pp. 567-572.
`doi:10.1016/j.ifacol.2015.06.141`

[11] A. Cerrone, J. Hochhalter, G. Heber, A. Ingraffea, On the effects of modeling as-manufactured geometry: toward digital twin, International Journal of Aerospace

Engineering, 2014 (Article ID 439278) (2014) pp. 1-10.
`doi:10.1155/2014/439278`

[12] M. Schluse, J. Rossmann, From simulation to experimentable digital twins: Simulation-based development and operation of complex technical systems, in 2016 IEEE International Symposium on Systems Engineering (ISSE) (2016) pp. 1-6.
`doi:10.1109/SysEng.2016.7753162`

[13] A. Canedo, Industrial IoT lifecycle via digital twins, in Proceedings of the Eleventh IEEE/ACM/IFIP International Conference on Hardware/Software Codesign and System Synthesis (2016) pp. 1-29.

[14] T. Gabor, L. Belzner, M. Kiermeier, M. T. Beck, A. Neitz, A simulation-based architecture for smart cyber-physical systems, in 2016 IEEE International Conference on Autonomic Computing (ICAC) (2016) pp. 374-379.
`doi:10.1109/ICAC.2016.29`

[15] J. Ríos, F. M. Morate, M. Oliva, J. C. Hernández, Framework to support the aircraft digital counterpart concept with an industrial design view, International Journal of Agile Systems and Management, 9 (3) (2016) pp. 212-231.
`doi:10.1504/IJASM.2016.079934`

[16] J. Lee, H. D. Ardakani, S. Yang, B. Bagheri, Industrial big data analytics and cyber-physical systems for future maintenance service innovation, Procedia Cirp, 38 (2015) pp. 3-7.
`doi:10.1016/j.procir.2015.08.026`

[17] J. Lee, B. Bagheri, H. A, Kao, A cyber-physical systems architecture for industry 4.0-based manufacturing systems, Manufacturing letters, 3 (2015) pp. 18-23.
`doi:10.1016/j.mfglet.2014.12.001`

[18] C. Legat, C. Seitz, S. Lamparter, S. Feldmann, Semantics to the shop floor: towards ontology modularization and reuse in the automation domain, IFAC Proceedings Volumes, 47(3) (2014) pp. 3444-3449.
`doi:10.3182/20140824-6-ZA-1003.02512`

[19] N. Jazdi, Cyber physical systems in the context of Industry 4.0, in: 2014 IEEE international conference on automation, quality and testing, robotics, Cluj-Napoca, 2014, pp. 1-4.
doi:10.1109/AQTR.2014.6857843

[20] M. Garetti, L. Fumagalli, E. Negri, Role of ontologies for CPS implementation in manufacturing, Management and Production Engineering Review, 6 (4) (2015) pp. 26-32.
doi:10.1515/mper-2015-0033

[21] E. Negri, L. Fumagalli, M. Garetti, L. Tanca, Requirements and languages for the semantic representation of manufacturing systems, Computers in Industry, 81 (2016) pp. 55-66.
doi:10.1016/j.compind.2015.10.009

[22] T. R. Gruber, Toward principles for the design of ontologies used for knowledge sharing?, International journal of human-computer studies, 43 (5-6) (1995) pp. 907-928.
doi:10.1006/ijhc.1995.1081

[23] S. Borgo, An ontological approach for reliable data integration in the industrial domain, Computers in Industry, 65 (9) (2014) pp. 1242-1252.
doi:10.1016/j.compind.2013.12.010

[24] S. Heymans et al. Ontology Reasoning with Large Data Repositories, in: M. Hepp, P. De Leenheer, A. De Moor, Y. Sure (eds) Ontology Management. Computing for Human Experience, vol 7. Springer, Boston, 2008, pp. 89-128.
doi:10.1007/978-0-387-69900-4_4

[25] J. Davis, T. F. Edgar, J. Porter, J. Bernaden, M. Sarli, Smart manufacturing, manufacturing intelligence and demand-dynamic performance, Computers Chemical Engineering, 47 (2012) pp. 145-156.
doi:10.1016/j.compchemeng.2012.06.037

[26] J. Lee, H. A. Kao, S. Yang, Service innovation and smart analytics for industry 4.0 and big data environment, Procedia Cirp, 16 (2014) pp. 3-8.
doi:10.1016/j.procir.2014.02.001

[27] E. Negri, L. Fumagalli, M. Macchi, A review of the roles of digital twin in cps-based production systems, Procedia Manufacturing, 11 (2017) pp. 939-948.
`doi:10.1016/j.promfg.2017.07.198`

[28] Representation of process control engineering requests in PI Diagrams and for data exchange between PID tools and PCE-CAE tools, IEC PAS 62424:2006 (2006).

[29] G. N. Schroeder, C. Steinmetz, C. E. Pereira, D. B. Espindola, Digital twin data modeling with automationml and a communication methodology for data exchange, IFAC-PapersOnLine, 49 (30) (2016) pp. 12-17.
`doi:10.1016/j.ifacol.2016.11.115`

[30] K. Gopalakrishnan, S. K. Khaitan, A. Choudhary, A. Agrawal, Deep Convolutional Neural Networks with transfer learning for computer vision-based data-driven pavement distress detection, Construction and Building Materials, 157 (2017) pp. 322-330.
`doi:10.1016/j.conbuildmat.2017.09.110`